View metadata, citation and similar papers at core.ac.uk

brought to you by CORE

provided by Clemson University: TigerPrints

Clemson University
TigerPrints

All Theses | Theses

5-2008

SYNthesis AND DIELECTRIC PROPERTIES OF NANOCRYSTALLINE BARIUM TITANATE AND SILVER/BARIUM TITANATE PARTICLES

Hiroki Maie
Clemson University, hmaie@clemson.edu

Follow this and additional works at: https://tigerprints.clemson.edu/all_theses

 Part of the Materials Science and Engineering Commons

Recommended Citation
Maie, Hiroki, "SYNthesis AND DIELECTRIC PROPERTIES OF NANOCRYSTALLINE BARIUM TITANATE AND SILVER/BARIUM TITANATE PARTICLES" (2008). *All Theses*. 305.
https://tigerprints.clemson.edu/all_theses/305

This Thesis is brought to you for free and open access by the Theses at TigerPrints. It has been accepted for inclusion in All Theses by an authorized administrator of TigerPrints. For more information, please contact kokeefe@clemson.edu.

SYNTHESIS AND DIELECTRIC PROPERTIES OF NANOCRYSTALLINE BARIUM TITANATE AND SILVER/BARIUM TITANATE PARTICLES

A Thesis
Presented to
the Graduate School of
Clemson University

In Partial Fulfillment
of the Requirements for the Degree
Master of Science
Material Science and Engineering

---

by
Hiroki Maie
May 2008

Accepted by:
Dr. Burtrand I. Lee, Committee Chair
Dr. Jian Luo
Dr. Eric C. Skaar

ABSTRACT

The increasing needs for further functionality, higher performance, and miniaturization of electronic devices have highly demanded down-size and volume-efficiency of electronic components such as multilayer ceramic capacitors (MLCCs). To meet this demand, the use of high dielectric constant material with nanometer size and spherical shape is considered as requirements. Embedded capacitors are an important emerging technology for meeting the performance and functionality requirements of next-generation electronic devices. One major obstacle for implementing this technology is the scarcity of dielectric materials with appropriate dielectric and mechanical properties was mainly discussed

Considering these backgrounds, this research is devoted to synthesis of high dielectric constant materials, barium titanate ($BaTiO_3$) nano-powders and silver/barium titanate ($Ag/BaTiO_3$) nano-composite powders for the applications of MLCCs and embedded capacitors. A noble synthesis method, ambient conditions sol (ACS) process, which was developed in our lab, has been further investigated to produce desirable $BaTiO_3$ and $Ag/BaTiO_3$ powders. ACS process was divided into two processes, depending on the synthesis medium, water-based ambient condition sol (WACS) process and solvent-based ambient condition sol (SACS) process. In WACS, water is used as a main medium, while in SACS, large amount of organic solvent in aqueous solution or totally organic solvent without water is used.

For the first part, nanocrystalline $BaTiO_3$ particles were prepared by WACS process. The effects of different processing parameters such as the concentration of Ba^{2+} ions and base and reaction time on the properties of the powders were investigated. In this work, how the content of the OH^- defects in $BaTiO_3$ lattices affect the tetragonality in a powder and dielectric constant was mainly discussed

For the second part, nanocrystalline $BaTiO_3$ particles were prepared by SACS process. The effects of the concentration of an organic solvent in a mixed solvent on the properties were investigated.

For the last part, $Ag/BaTiO_3$ nanocomposites were directly synthesized via an ambient condition sol (ACS) process. The properties of the composite powders were studied in relation to temperature of heat-treatment and Ag concentration.

DEDICATION

I dedicate this work to my father, mother, and grandparents in appreciation of their love, support and encouragement, which helped me reach this stage.

ACKNOWLEDGEMENTS

I would like to take this opportunity to thank all of the people who made this thesis possible. Sincere gratitude is extended to my advisor, Dr. Burtrand I. Lee, for his scientific guidance in academic affairs and advice in personal matters. He really does deserve the greatest of thanks, since he has provided me with incredible support, encouragement, advice, as well as guidance in conducting the research. I am also grateful to my committee members: Dr. Jian Luo and Dr. Eric C. Skaar for accepting to serve on my committee, and I especially thank them for taking time to read this dissertation and provide critical evaluation of my work.

I would like to thank Mr. Greg Schlock, Mrs. Kimberly Ivey, and Mr. Don for their analytical support and technical advice. I am grateful to all my colleagues in Dr. Lee's research group; Gopi, Ravi, Sujaree, Daniel, Dr. Jin and Dr. Ali, for their words, help and suggestions that boosted my courage.

Finally, I want to thank my father (Hideo Maie), mother (Atsuko Maie), and grandparents for their continuous support and encouragement. Without them, I could not even finish this thesis.

TABLE OF CONTENTS

Table of Contents (Continued)

Page

Table of Contents (Continued)

Page

LIST OF TABLES

LIST OF FIGURES

List of Figures (Continued)

Figure Page

List of Figures (Continued)

Figure Page

CHAPTER 1

INTRODUCTION

1.1 Structure and Dielectric Property of $BaTiO_3$

$BaTiO_3$, due to its excellent dielectric properties, is one of the most widely used ceramic materials in the electronic ceramic industry. Also $BaTiO_3$ is environmentally harmless and a relatively cheap material comparing with PZT or PMN-PT.

$BaTiO_3$ has a typical perovskite structure, which is shown in Figure 1.1. Perovskite materials, with a general stoichiometry of ABO_3, represent a unique class of crystalline solids that demonstrate a variety of interesting dielectric, piezoelectric, ferroelectric, and electro-optic properties. The unique properties of perovskite materials are the result of the crystal structure, phase transitions as a function of temperature, and the size of the ions present in the unit cell.

Above it's Curie point (about 130 °C), the unit cell of $BaTiO_3$ is cubic as shown in Fig. 1.1 [1]. The barium (Ba) ions reside at the corners of the cubic forming a close-packed structure along with the oxygen (O) ions, which occupy the face centers of the cubic. Each Ba ion is surrounded by twelve O ions, and each O ion is surrounded by four Ba ions and eight O ions. In the center of the face-centered cubic unit cell, the small highly charged titanium (Ti^{4+}) ion is octahedrally coordinated by six oxygen ions.

The lattice parameter of $BaTiO_3$ is slightly larger than that of the ideal perovskite due to the size of Ba ions. Because of the large size of the Ba ions, the octahedral

interstitial position in $BaTiO_3$ is quite large compared to the size of the Ti ions. To some extent, the Ti ions are too small to be stable in these octahedral positions and tend to shift themselves to an off-centered position resulting in an electric dipole. Since each Ti ion has a + 4 charge, the degree of the polarization is very high [2]. When an electric field is applied, Ti ions can shift from random to aligned positions and result in high bulk polarization and a high dielectric constant.

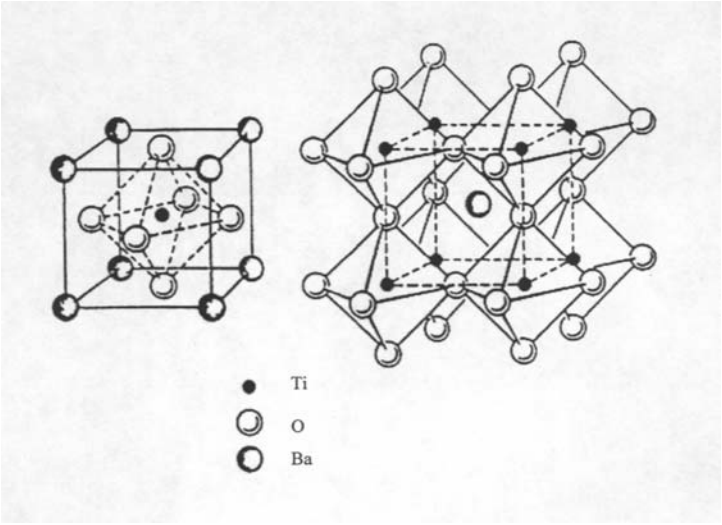

Fugure 1.1 Perovskite structure of $BaTiO_3$

The crystal structure and dielectric characteristics of $BaTiO_3$ strongly depend on temperatures. When the temperature is below the Curie temperature, the cubic structure is slightly distorted to a ferroelectric tetragonal structure having a dipole moment along the c direction [1, 2]. When the temperature goes down below 0 ^oC, the tetragonal structure will transform to an orthorhombic ferroelectric phase with the polar axis parallel to a face diagonal. When the temperature is reduced further to -80 ^oC, it will transform to a

rhombohedral structure with the polar axis along a body diagonal. All of the phase transformations of $BaTiO_3$ single crystal are illustrated in Fig. 1.2. The temperature dependence of the relative permittivity of $BaTiO_3$ measured in the a and c directions is shown in Fig. 1.3.

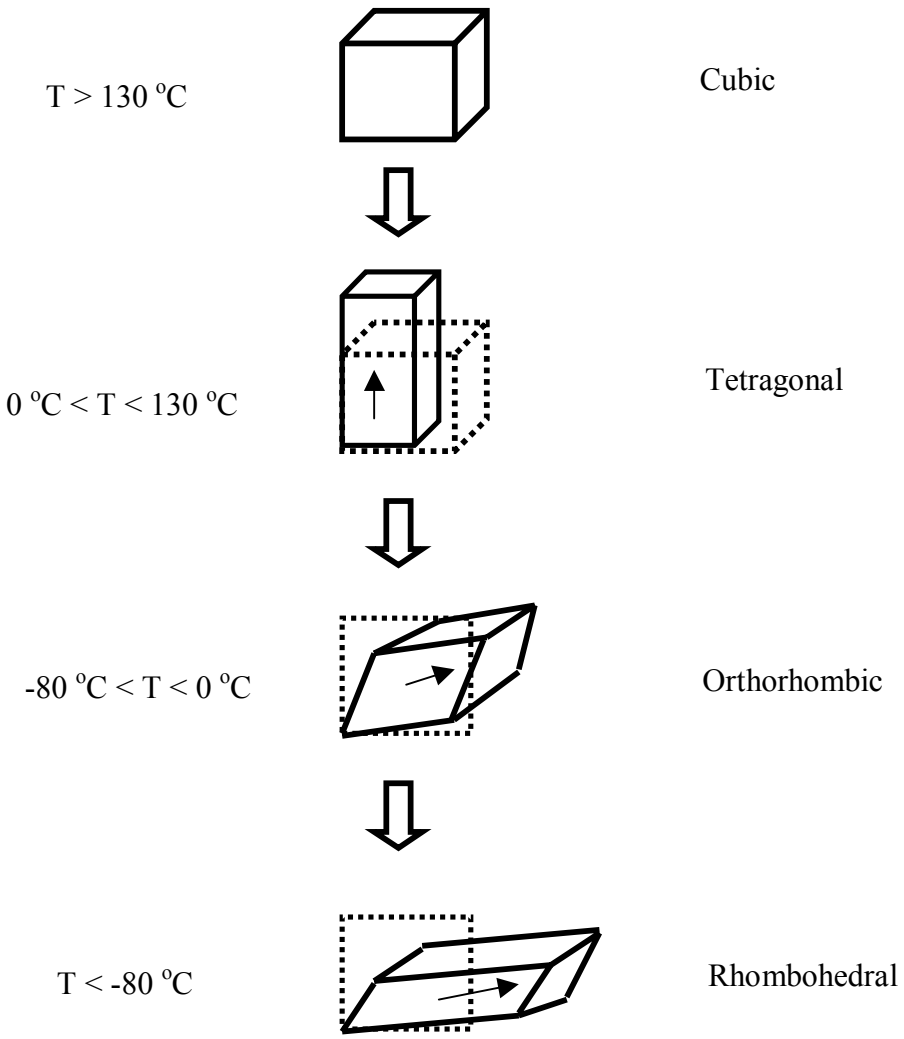

Figure 1.2 Phase transformations of the $BaTiO_3$ crystal at different temperatures

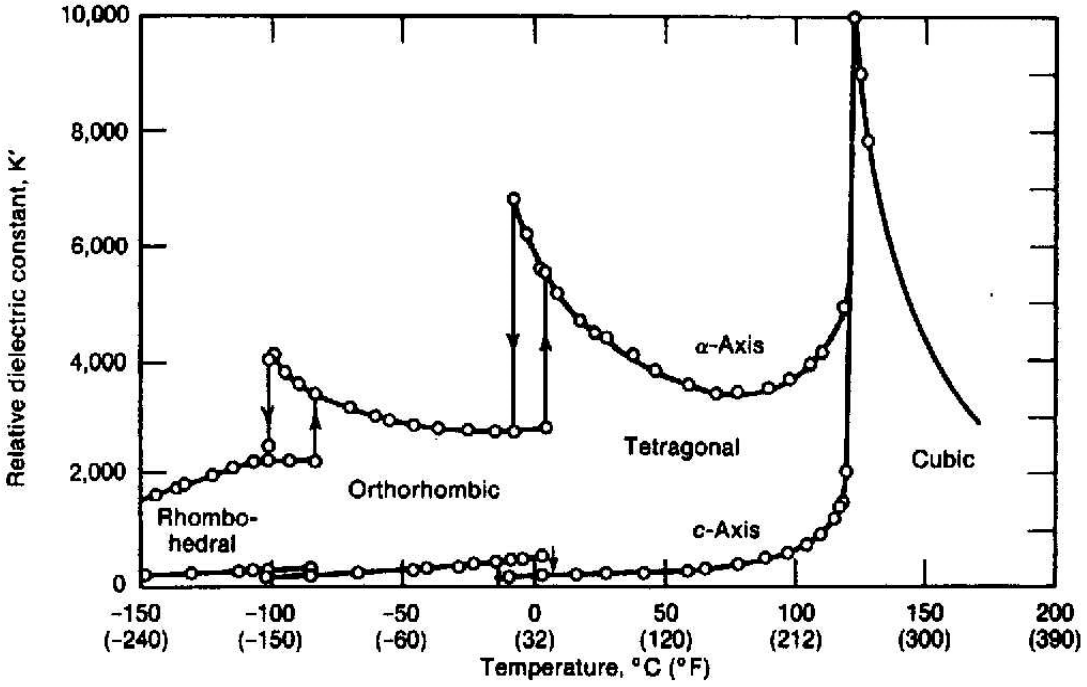

Figure 1.3 Temperature dependence of relative permittivity of $BaTiO_3$ single crystal

1.2 Multilayer Ceramic Capacitor (MLCC)

The MLCC structure (Figure 1.4) enables the maximum capacitance available by packing many thin dielectric layers into a limited space. The capacitance (C) of each ceramic layer is proportional to the thickness (d) of the layer according to the equation 1.1:

$$C = k\varepsilon_0 \frac{A}{d} \qquad [1.1]$$

where k is the dielectric constant of the ceramic material, ε_0 is the permittivity of free space (8.85×10^{-12} F/m), and A is the area of each layer [1]. The total capacitance of a

MLCC is equal to the sum of the individual layers, where n is the number of ceramic layers.

$$C_{MLCC} = \mathrm{n} \times \mathrm{C}_{Each\ layer} = k\varepsilon_0 \frac{nA}{d} \qquad [1.2]$$

Equation 1.2 indicates that an increase in the number of ceramic layers (n) can increase the capacitance of MLCC. Therefore, for a given size of MLCC, thinner layers and a higher dielectric constant of ceramic material are desirable.

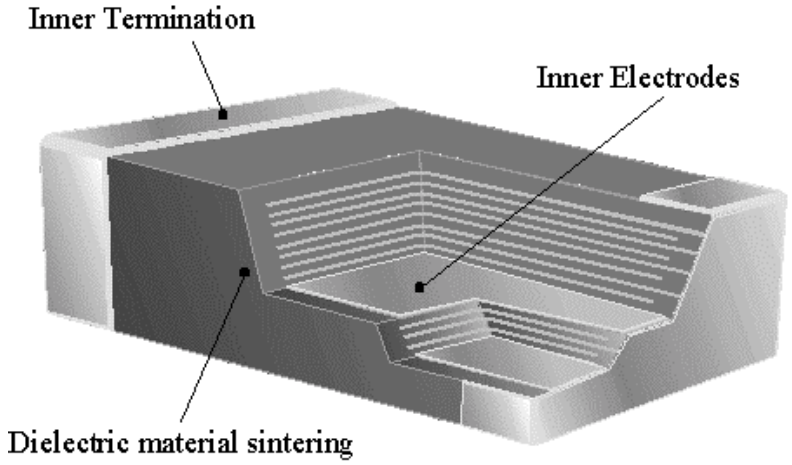

Figure 1.4 Schematic 3-dimensional view of the MLCC

The MLCC industry is continuing intensive efforts to reduce component size, decrease layer thickness and improve component reliability [3]. Up to now, the state-of-the-art layer thickness is below 2 μm, but it is expected that layers as thin as 1 μm layer or less will be available with the next generation of components [4]. To achieve that goal,

the use of nano-sized (~100 nm) $BaTiO_3$ particles with narrow particle size distribution (PSD), controlled morphology, and high dielectric constant are preferred.

1.3 Synthesis Process

Over the past years, many methods have been proposed to produce $BaTiO_3$ powders. Conventionally, $BaTiO_3$ powder was prepared by a solid-state reaction method [5-7] through heating $BaCO_3$ and TiO_2 to temperatures as high as 1100-1200 ^oC. This method, however, leads to large $BaTiO_3$ particles (usually above 1 μm) with wide grain-size distribution, irregular morphologies and impurities, which may result in poor electrical properties and reproducibility of sintered ceramics. To obtain finer $BaTiO_3$ powders with high quality, many synthesizing methods have been developed. Among those methods, a sol-gel method [8-10] and hydrothermal synthesis [11-14] are the most widely used methods for nanocrystalline $BaTiO_3$ synthesis. In the sol-gel process, $BaTiO_3$ gels can be obtained by hydrolyzing the metal alkoxide. The most advantageous characteristics of this method are the high purity and the excellent control of the composition of the resulting powders. To crystallize $BaTiO_3$, however, the hydrolysis product should normally be calcined at temperature above 500^oC. The expensive raw materials and the low yield rate are the main hindrances for the commercial application of this method. In contrast to this, hydrothermal synthesis can lower the processing temperature. This technique involves heating an aqueous suspension or slurry of reactants in an autoclave (pressure vessel) at a moderate temperature, (e.g., below 300 ^oC), and pressure so that the

crystallization of a desired phase will take place. Cheaper starting precursors are frequently used, such as barium hydroxide or barium chloride and titanium oxide or titanium chloride. This process produces fine $BaTiO_3$ powders (<300nm) with narrow size distribution, high crystallinity, and high purity. The advantages of hydrothermal crystallization are the reduced energy costs due to the moderate temperatures sufficient for the reaction, simplicity in the synthesis process, and the enhanced rate of the precipitation reaction.

Recent interest has been focused on the direct precipitation of $BaTiO_3$ in aqueous or mixed organic-aqueous media at lower temperatures (<150^oC) and ambient pressure. To meet this trend and develop a synthesis process for large-scale commercial production, our novel synthesis method, ACS method [15-19] has been used. Comparing with hydrothermal method, an ACS process does not require an autoclave, and the synthesis process is conducted in water-based solvent or in a mixed solvent of alcohol and water under mild conditions.

1.4 Impurities and Defects in $BaTiO_3$

Carbonates and hydroxyl groups are the main impurities and defects in $BaTiO_3$ powders. It is likely that $BaCO_3$ is formed during the synthesis of $BaTiO_3$ powder, whichever route is used [20]. Incomplete reaction of $BaCO_3$ or excess of $BaCO_3$ leads to $BaCO_3$ impurity in the $BaTiO_3$ powders prepared by solid state reaction [20]. The hydrothermal synthesis of $BaTiO_3$ is based on the aqueous reaction between Ba and Ti

species at a high pH. $BaCO_3$ is always formed as a byproduct due to the atmospheric absorption of CO_2 and the high thermodynamic stability of $BaCO_3$ at high pHs in aqueous solutions [21]. However, $BaCO_3$ can be removed by washing $BaTiO_3$ powders with dilute acid solution [14].

Clark et al. [22] reported that as-prepared hydrothermal $BaTiO_3$ contained many defects, primarily in the form of lattice OH^- ions. By studying the defects and microstructure of hydrothermal $BaTiO_3$, Hennings et al. [23] pointed out that, in correspondence to the high amount of lattice OH^- ions, a large amount of protons existed in the oxygen sublattice. In addition, existence of hydroxyl defects in the perovskite lattices can result in enlarged unit cell volume [24, 25], which causes a suppression of the tetragonal distortion of the perovskite unit cell at room temperature.

1.5 Ferroelectric Ceramic - Metal composites

Recently, ferroelectric ceramic-metal composites have been of great interest and a lot of research on these composite systems has been carried out, reporting a high increase in the dielectric properties of the ceramics [6-10]. Yuanhua et al. [6] have reported that the dielectric constant of $Na_{0.5}Bi_{0.5}TiO_3$ (NBT) based composites incorporating silver particles could be enhanced up to ~20 times higher than that of pure NBT. Pecharroman et al. [7] studied the dielectric properties of $Ni/BaTiO_3$ composites and reported a modest increase in dielectric constant for lower vol.% of Ni. But this ratio reached the

percolation threshold of 30 vol%, an ultra high room temperature dielectric constant of K = 80000 was attained. This percolation threshold will be explained in the next section.

1.5.1 Percolation for Dielectrics

All materials will polarize more or less within an electric field. The induced dipole moment is decided by materials's polarizability as shown in Eq. 3.1:

$$\vec{\mu} = \alpha \cdot \vec{E} \tag{3.1}$$

where, $\vec{\mu}$ is the induced dipole moment; α and $\vec{E}$ are the polarizability of materials and electrical strength, respectively. The dielectric constant of materials is related to its polarizability at a certain temperature and frequency. The higher the polarizability is, the higher the dielectric constant will be.

In $BaTiO_3$, since the size of Ti^{4+} cation is smaller than the interspace of the oxygen octahedron that surrounds it, $BaTiO_3$ can be polarized by the displacement of Ti^{4+} from the oxygen octahedron center to an off-center position. Because of the high concentration and high valence of Ti^{4+} in $BaTiO_3$, $BaTiO_3$ can show great macroscopic polarization (with dielectric constants > 1000), if a significant amount of Ti^{4+} displacements are aligned.

Metal particles, when insulated from electrodes, can be polarized by an electric field in the same way as dielectric ceramics or any other material. The only difference is that the polarization is caused by the displacement of free electrons rather than ions. When the concentration of metal fillers increases, not only the total polarization increased, but also

the coupling of polarization between filler particles is enhanced because the distance between metal particles decreases. This is the main mechanism in which metal-ferroelectric ceramic composites showed increased dielectric constants. However, according to the percolation theory [2-5], it is known that at a metal concentration near the percolation threshold, the dielectric constant will show a spike-like increase, but beyond it, the dielectric constant will sharply decrease to almost zero and dielectric loss will become extremely high. Thus, although this polarization of metal particles can successfully contribute to the enhancement of the dielectric constant of the ceramics and a quite high dielectric constant can be expected near the percolation threshold, the risk of percolation and high loss should be considered for practical applications.

1.6 References

1. J. Moulson and J. M. Herbert, "Electronic Ceramics: Materials, Properties and Applications," Chapman & Hall, New York, (1990)
2. D. W. Richerson, "Modern Ceramic Engineering," Marcel Dekker, New York, (1992)
3. J. M. Wilson, Am. Ceram. Soc. Bull. **74** (6) 106 (1995)
4. C. Pithan, D. Hennings and R. Waser, Int. J. Appl. Ceram. Technol. **2** [1] 1 (2005)
5. A. Bauger, J. C. Mutin, and J. C. Niepce, J. Mater. Sci., **18** 3041 (1983)
6. M. S. H. Chu and A. W. I. M. Rae, Am. Ceram. Soc. Bull., **74** [1-2] 69 (1995)
7. P. P. Phule and S. H. Risbud, J. Mater. Sci., **25** 1169 (1990)
8. M. H. Frey and D. H. Payne, Chem. Mater., **7**, 123 (1995)

9. H. Shimooka and M. Kuwabara, J. Am. Ceram. Soc., **79** [11] 2983-2985 (1996)

10. B. I. Lee and J. P. Zhang, Thin Solid Films, **388** [1-2] 107 (2001)

11. R. Vivekanandan and T. R. N. Kutty, Powder Technology, **57** 181 (1989)

12. C. T. Xia, E. W. Shi, W. Z. Zhong, and J. K. Guo, J. Euro. Ceram. Soc., **15** 1171 (1995)

13. P. K. Dutta, R. Asiaie, S. A. Akbar, and W. D. Zhu, Chem. Mater., **6** 1542 (1994)

14. S. W. Lu. B. I. Lee, Z. L. Wang, and W. D. Samuels, J. Crystal Growth, **219** 269 (2000)

15. X. Wang, B.I. Lee, M.Z. Hu, E.A. Payzant and D.A. Blom, J. Mater. Sci. Lett. **22** 557 (2003)

16. X. Wang, B.I. Lee, M.Z. Hu, E.A. Payzant and D.A. Blom, J. Mater. Sci. – Mater. Electron. **14** 495 (2003)

17. X. Wang, B.I. Lee, M. Hu, E.A. Payzant and D.A. Blom, J. Euro. Ceram. Sci. **26** 2319 (2006)

18. N.G. Devaraju, B.I. Lee, M. Viviani, P. Nanni and E.S. Kim, J. Mater. Sci. **41** 3335 (2006)

19. B.I. Lee, X. Wang, S.J. Kwon, H. Maie, R. Kota and J. H. Hwang, J. G.. Park, M. Hu, Microelectron. Eng. **83** 463 (2006)

20. M. C. B. Lopez, G. Fourlaris, B. Rand, and F. L. Riley, J. Am. Ceram. Soc., **82** [7] 1777 (1999)

21. M. M. Lencka and R. E. Riman, Chem. Mater., **5** 61 (1993)

22. I. J. Clark, T. Takeuchi, N. Ohtori, and D. Sinclair, J. Mater. Chem., **9** 83 (1999)

23. D. F. K. Hennings, C. Metzmacher and B. S. Schreinemacher, J. Am. Ceram. Soc., **84** [1] 179 (2001)

24. G. Busca, V. Buscaglia, M. Leoni, and P. Nanni, Chem. Mater. **6** 955 (1994)

25. J. G. Lisoni, F. J. Piera, M. Sanchez, C. F. Soto and V. M. Fuenzalida, Applied Surface Science, **134** 225 (1998)

CHAPTER 2

THE HYDROXYL CONCENTRATION AND THE DIELECTRIC PROPERTIES OF BARIUM TITANATE NANO-POWDER SYNTHESIZED BY WATER-BASED AMBIENT CONDITION SOL PROCESS

Abstract

Nanocrystalline barium titanate, $BaTiO_3$, powders have been successfully synthesized via water-based ambient condition sol (WACS) process, using barium hydroxide and titanium isopropoxide. The properties of the powder were investigated as a function of various processing parameters such as the concentration of Ba^{2+} ions ($[Ba^{2+}]$), the concentration of base, and reaction time. The concentration of hydroxyl (OH^-) groups in the $BaTiO_3$ powder was greatly affected by changing the values of each processing parameter. The dielectric constant and tetragonality of the powders which contain lattice OH^- more than 0.35 wt% were little affected with further increase in the lattice OH^- concentration. The dielectric loss was highly varied with the concentration of the OH^- groups, and it was increased with increasing OH^- concentration. Calcination treatment significantly improved the dielectric properties of the powder. With higher calcination temperature, the dielectric constant increased and the dielectric loss decreased.

1. Introduction

$BaTiO_3$, owing to its high dielectric constant and low losses, is the most widely used dielectric material for electronic ceramic capacitors such as MLCCs and embedded capacitors in printed circuit boards (PCB).

With recent advances in electronic devices and communications, the miniaturization and higher volumetric efficiency of MLCC have been highly demanded by electronic industries. These requirements are, in general, achieved by reducing the thickness of dielectric layers or increasing the number of the dielectric layers in MLCCs. MLCCs with a dielectric thickness below 2 μm have already been commercialized recently, but it is expected that layers as thin as 1μm or less will be available [1]. Consequently, the particle size of raw material, $BaTiO_3$, will continue to decrease to a few tens of nm for this application.

As another application, fine $BaTiO_3$ particles are needed as filler which are incorporated and dispersed in a polymer. This polymer-matrix composite with dielectric ceramic powder is quite common in embedded capacitors [2-5]. However, in most cases, these composites suffer a low relative dielectric constant even with high filler loading (>50 vol%) [6]. In fact, this low performance of the composite is mainly because of the low dielectric constant of polymer [6], but it is quite important to use ceramic powder with high dielectric constant for the further enhancement of the dielectric properties. Using a fine $BaTiO_3$ powder with tetragonal phase or high tetragonality should be the key to achieve great dielectric properties of this composite.

To meet the desires mentioned, a lot of methods to synthesize fine $BaTiO_3$ powder have already been proposed and studied. Among them, a hydrothermal process [7-13] has been considered as a powerful method for direct preparation of fine and homogeneous $BaTiO_3$ powders without high temperature calcination and ball-milling.

However, it is well known that $BaTiO_3$ nanopowders prepared by the hydrothermal process have significant concentration of OH^- defects in the lattice [14-17]. These OH^- ions in hydrothermal powders are located on the oxygen sites in the perovskite lattice. The cationic vacancies (vacancies on metal sites) must be formed to maintain charge neutrality in the perovskite lattice. These OH^- and cationic defects, in general, impart adverse effects on the properties of the powder as well as on sintering. For example, these defects cause intragranular pores to form in sintering because of the disappearance of OH^- defects as H_2O. In MLCCs, these intragranular pores are preferentially collected at the inner electrodes, which results in bloating, cracks, and delamination [14]. According to X-ray diffraction (XRD) pattern, the crystal structure of hydrothemally prepared nanosize $BaTiO_3$ nanopowder, in general, is cubic phase at room temperature. The main reason for this room temperature stabilization of the cubic structure is due to the lattice strain associated with the presence of lattice OH^- ions and cationic vacancies, which means that the lattice strain existing in the perovskite lattices hinders the conversion of crystal structure from cubic to tetragonal phase. Therefore, in order to produce fine powder with less entrapped OH^-s and high tetragonality, an investigation on how the processing parameters affect OH^- concentration in $BaTiO_3$ is important to study.

In this work, the WACS method [18-22] was used for preparation of fine $BaTiO_3$ powders with the desired properties, which is the direct precipitation process of $BaTiO_3$ in aqueous medium under relatively mild conditions. The effects of the processing parameters and heat treatment on the properties of the powder such as crystallite and particle size, OH^- concentration and dielectric properties were investigated. Particularly, special attention was paid to the OH^- concentration and dielectric properties of the powders, and their relationship.

2. Experimental

2.1. Powder synthesis

Barium hydroxide (Chemical Products Corporation, Cartersville, GA) and titanium isopropoxide (Tyzor TPT, Dupont chemical solutions enterprise, Wilmington, DE) were used as the starting materials. Barium hydroxide was dissolved in distilled water at room temperature by stirring in a 500 ml Teflon jar to form solution A. Solution B was formed by dissolving titanium isopropoxide in isopropanol (Alfa Aesar, 99.5%) with stirring. Solution B was slowly added to solution A with constant stirring. The volume ratio of isopropanol/H_2O is 0.06. The Ba/Ti precursor molar ratio in the mixture solution was kept constant at 1.3. The Ba^{2+} ion concentration ($[Ba^{2+}]$) was varied from 0.1 to 0.7M. Tetramethyl ammonium hydroxide (TMAH) (25% w/w aq. soln. Alfa Aesar) was used as the base and it was slowly added into Ba and Ti mixture solution with vigorous stirring before heating. The TMAH concentration was varied from 0 to 1.82M. The resulting

white slurry was then heated to 120 ^{o}C for reaction times ranging from 0 to 24 hours while stirring in an oil bath. The resulting precipitate solids were repeatedly washed with distilled water to get rid of extra barium ions. These products were dried overnight at 80 ^{o}C in a vacuum oven and the dried lumps were crushed.

To investigate the effects of heat treatment, it was performed under mild calcination temperature between 200 and 700 ^{o}C for 4 hrs, using the powder synthesized for 4hrs in the solution containing TMAH concentration of 1.46M and [Ba^{2+}] of 0.2M.

2.2. Powder characterization

The all prepared samples were examined by XRD. Room temperature XRD patterns of $BaTiO_3$ were recorded in the 2θ range of 20^{o} - 80^{o}, 37^{o} - 40^{o}, and 44^{o} - 47^{o} (RTXRD, Scintag PADV using CuK_{α} with λ=0.15406 nm). The crystallite size of $BaTiO_3$ was calculated from the (110) peak of the corresponding XRD pattern using Scherrer equation, $D=0.9\lambda/\beta\cos\theta$, where λ is the wavelength, θ is the angle of diffraction, and β is the full-width at half maximum (FWHM). The a-axis was also calculated using the (110) peak of XRD on the assumption that the crystal structure is cubic phase. To evaluate the tetragonality in a powder, the c/a ratio was obtained based on the (200) peak of XRD. Microcal Origin software was used for the calculation by deconvoluting the (200) peak into two separate ones. The specific surface areas (S_{BET}) were measured by a BET surface area analyzer (Micromeritics ASAP 2020 automated system). The average particle size was calculated from the measured specific surface area by using the following equation,

$d_{BET}=6/(\rho S_{BET})$, where ρ is the density of $BaTiO_3$. The microstructure, particle size, and the morphology of $BaTiO_3$ powders were investigated by a transmission electron microscope (TEM) (Hitachi, HD2000). To evaluate the OH^- group content in the powders, a fourier transform infrared spectrometer (FT-IR) (Nicolet Magna-IR 550) and thermal gravimetric analysis (TGA) (Perkin Elmer TGA-7 Thermogravimetric Analyzer) were used.

The dielectric constants of the powders were characterized by measuring the capacitance of the particle composites. The capacitor was fabricated using a procedure described elsewhere [22-23] using castor oil as the matrix with 30vol% of powder in the slurry paste form, which filled the Teflon-cell with aluminum plate electrodes. Capacitance was measured at 1 MHz using an LCR meter (HP 4284A Precision LCR Meter). The dielectric constant values (K) of the capacitors were calculated from the measured capacitance data using the equation: $C=K\varepsilon_o A/t$, where ε_o is the dielectric permittivity of the free space, ($8.854*10^{-12}$ F/m), A is the contact area between the electrode and composite paste, ($1cm^2$), and t is the thickness of the ceramic specimen, (0.4 cm). The measured dielectric constant of the capacitor with only castor oil was 4.9 and it was close to that of the literature value of castor oil, 4.7.

3. Results and Discussion

3.1. [Ba^{2+}] effect

The effects of Ba^{2+} ion concentration in the starting solution were examined. The results were obtained from powders reacted for 4 hrs in the solution without adding the base, i.e. TMAH. The [Ba^{2+}] was varied from 0.1 to 0.7M. In this precipitation process, barium hydroxide octahydrate is used not only as Ba source, but also as the supplier of OH^- ions in the aqueous solution to make a basic condition. Thus, the proper concentration for synthesis of the powder needs to be known. Fig. 2.1 shows the room temperature XRD patterns of the $BaTiO_3$ powders. According to Fig.2.1, at [Ba^{2+}]=0.1M, relatively small peak of $BaTiO_3$ were seen, In addition, the amorphous phase between (100) and (111) and $BaCO_3$ phase were also observed. The presence of amorphous phase implies that the crystallization is still in the process. This should be because of the slow crystallization speed at [Ba^{2+}]=0.1M. For the full crystallization, longer reaction time or higher reaction temperature should be required at [Ba^{2+}] =0.1M. When [Ba^{2+}] is higher than 0.1M, the sharp peaks for $BaTiO_3$ phase and the small peak for $BaCO_3$ phase were observed as shown in Fig.2.1. The crystal structure of $BaTiO_3$ was assigned to the cubic phase because the (200) and (002) peaks around $2\theta = 44.95^o$ were not split. With increasing [Ba^{2+}] concentration, the XRD peak intensities decreased while the full width at half-maximum (FWAH) values were increased. This means that the formed nanocrystals tend to become smaller. In fact, Fig. 2.2 shows that the crystallite and particle size were decreased with increasing [Ba^{2+}] concentration. The particle size becomes close to the crystallite size with increasing [Ba^{2+}] concentration, indicating that the particles synthesized at a high [Ba^{2+}] concentration are composed of fewer

crystallites. These phenomena can be understood by considering a change in the nucleation and crystallite growth for the formation of the nanocrystalline particle. The size of the particles that precipitate out of solution depends, in general, on the relative rates of nuclei formation and crystallite growth [24-26]. The high nucleation rate condition can produce a large number of small crystallites. For a given system, the rates of nucleation and growth depend on supersaturation. Supersaturation is affected by reactant concentration, temperature, and mixing conditions [24-26]. At higher values of [Ba^{2+}] concentration, a larger number of Ba^{2+} ions are diffusing in the solution and more Ba^{2+} ions react with titanium gel, leading to higher supersaturation of $BaTiO_3$ and higher nucleation rate. As a result, the size of the final particles decreases with increasing [Ba^{2+}] concentration while a large number of small crystallites are formed.

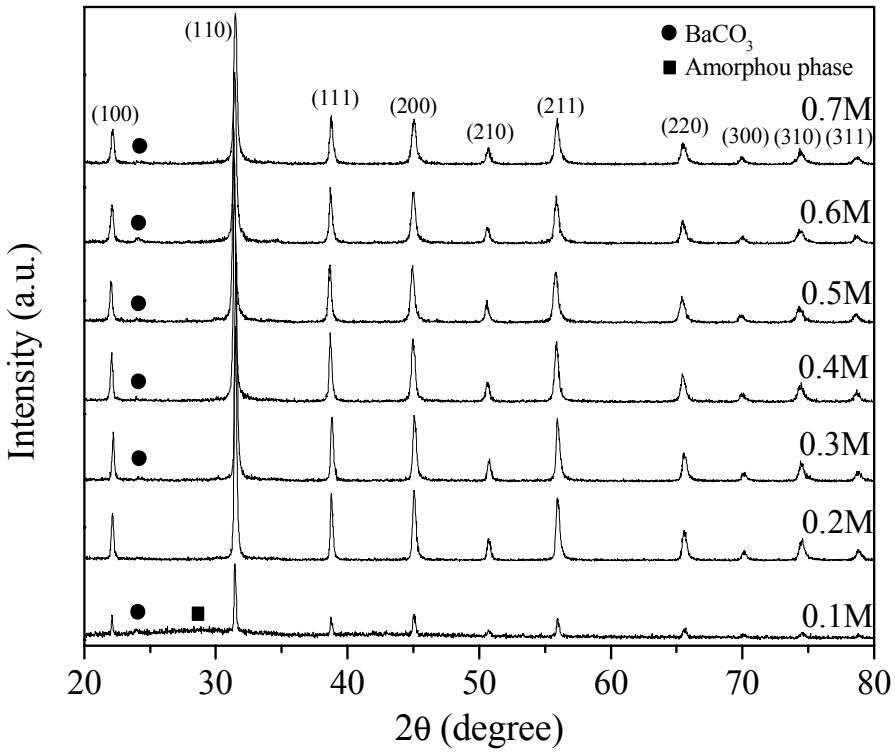

Figure 2.1 XRD patterns of $BaTiO_3$ powder synthesized by different values of the $[Ba^{2+}]$ concentration in the starting solution from 0.1 to 0.7M

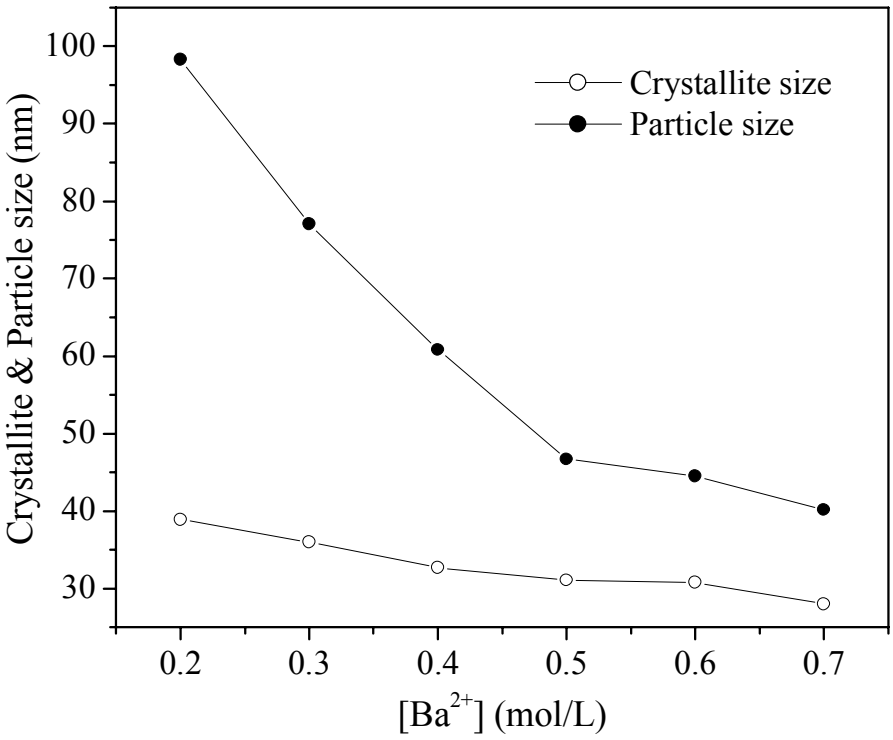

Figure 2.2 Crystallite and particle size of $BaTiO_3$ powders synthesized with $[Ba^{2+}]$ concentration in the starting solution

In order to estimate the OH^- content in the as prepared powders, semi-quantitative FT-IR analysis was performed by using the FT-IR baseline method and normalization [27-30]. All the FT-IR data for the samples showed a broad band in the very wide wave number region from 2500 to 3750 cm^{-1}, which is caused by the O-H stretching vibration [31-36]. This broad band is categorized into two main groups; lattice OH^- group and surface-absorbed OH^- group. The sharp absorption band peak around 3510 cm^{-1} in the broad region is assigned to O-H stretching vibration of the lattice OH^- group [32,35]. On the other hand, the band at 3200 cm^{-1} was used to estimate the surface OH^- content as the band of the surface OH^- group is broad. The strong peak seen around 535cm^{-1} is assigned to the band for the lattice vibrational mode of $BaTiO_3$ [36]. Measured OH^- band intensities were normalized by the band intensity of $BaTiO_3$. As a result, the band height ratios of I_{3510}/I_{535} and I_{3200}/I_{535} were used to estimate the relative content of both lattice and surface OH^- in $BaTiO_3$ particles. As shown in Fig. 2.3, the behavior of OH^- band ratios corresponds well to that of weight loss of OH^- groups during calcination between 100 and 700 ^oC measured with TGA. According to Fig. 2.3, the content of OH^- groups increased with high $[Ba^{2+}]$ concentration, and the increasing rate of OH^- groups slowed down at higher $[Ba^{2+}]$ concentration. With this increase in OH^- content, the a-axis in the unit lattice also increased from 0.4015 to 0.4028nm. This is because lattice OH^- groups expand and enlarge the unit lattices in $BaTiO_3$, which leads to the enlargement of the a-axis [16]. The weight loss from H_2O removal between RT and 100^oC measured with TGA increased from 0.08% to 0.62%. The contribution of the presence of H_2O to the

2500 to 3750 cm^{-1} region should be relatively small. Especially, the lattice OH^- peak at 3510 cm^{-1} should not be affected by the presence of H_2O.

Fig. 2.4 shows that the dielectric constant is not changed with [Ba^{2+}] concentration. This indicates that even though the particle size, crystallite size, OH^- content, and the a-axis in the unit lattice are all changed over the wide range with [Ba^{2+}] concentration, the dielectric constants are not affected by them in the range of their changes. The plausible reason for this should be that the tetragonality of all the samples was little changed with [Ba^{2+}] concentration. In fact, the c/a ratio, tetragonality, of the samples varied only between 1.0013 and 1.0018. This indicates that the range of the ratio is quite narrow as well as the tetragonalities of the samples are all quite low, which should have led to the stationary dielectric constants. Thus, it can be assumed that the dielectric constant is highly dependent on the tetragonality. On the other hand, it is observed that the dielectric loss is increased with higher [Ba^{2+}] concentration. This should be associated with the concentration of OH^- groups in the powder. The behavior of increasing dielectric loss in Fig. 2.4 agreed well with that of OH^- groups as shown in Fig. 2.3.

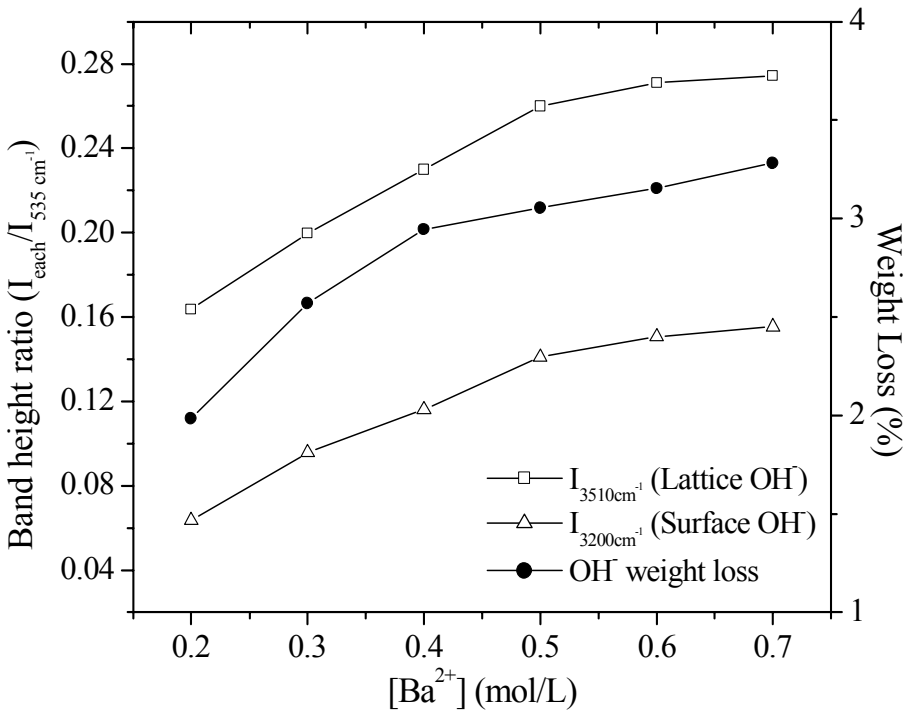

Figure 2.3 Normalized band height ratios of lattice and surface OH^- groups and weight loss of OH^- groups between 100 and 700 ^oC as a function of $[Ba^{2+}]$ concentration

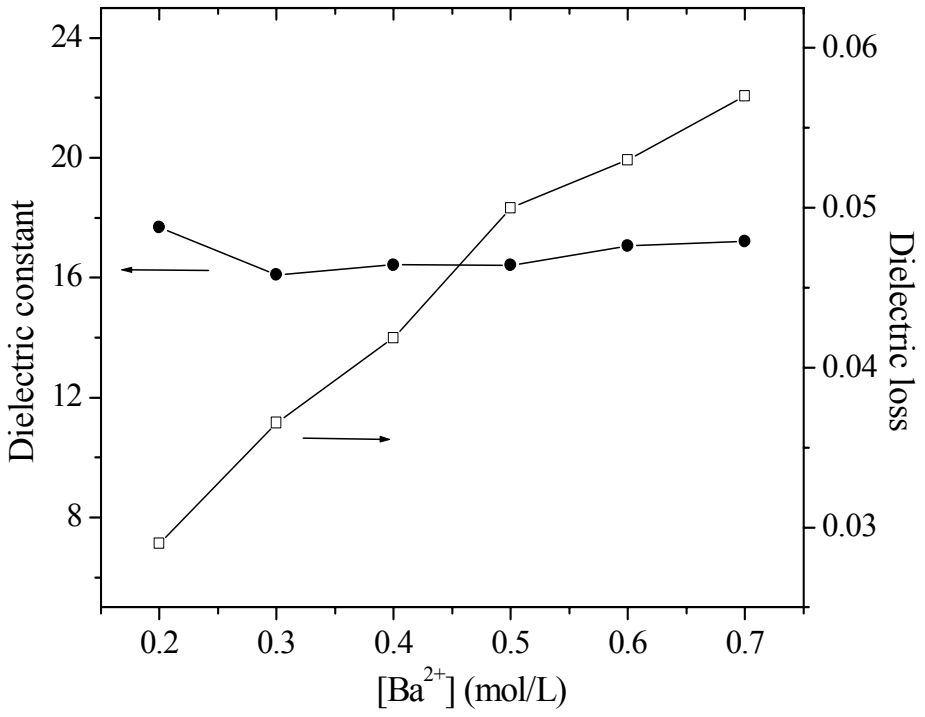

Figure 2.4 Room temperature dielectric constant and loss of castor oil-matrix composite with 30vol% of $BaTiO_3$ powder as a function of $[Ba^{2+}]$ concentration

3.2. Effect of basicity

The results in this section are obtained from $BaTiO_3$ powders synthesized for a reaction time of 4hrs in the solution containing [Ba^{2+}] of 0.2M and TMAH concentration of 0-1.82M. TMAH was chosen as the base because the common alkaline solution such as sodium or potassium hydroxide gives the contamination with Na^+ or K^+. They impart an adverse effect on the dielectric properties of the as-prepared powder. In fact, it is not necessary to add a basic solution in order to prepare fine $BaTiO_3$ powders according to the above result, if [Ba^{2+}] is higher than 0.1M. However, Xu et al. [12,13] reported that tetragonal $BaTiO_3$ powder with an average particle size of 70~80 nm was prepared by a hydrothermal process at a high pH and 240 ^oC for 12 hrs, using Ba and Ti chlorides. They claimed that OH^- ions seem to act as a catalyst by accelerating the transition of cubic-$BaTiO_3$ to form tetragonal $BaTiO_3$. Kwon et al. [37], on the other hand, reported a mixture solution of ethanol and water with no additional OH^- ions can produce fine $BaTiO_3$ powders with high tetragonality at 210 ^oC in an autoclave. This means that the fewer number of OH^- ions in the starting solution is effective for synthesis of high tetragonality $BaTiO_3$, but contradicts the results of Xu et al. Thus, the effect or role of OH^- concentration in the starting solution is important to study. In this study, the samples are prepared in the wide range of TMAH concentrations, but the peaks for the tetragonal phase were not observed according to the XRD data.

Fig. 2.5 indicates that the crystallite and particle size decreased with increasing TMAH concentration. This result implies that higher TMAH concentration promotes the

rate of nucleation over growth and dispersion. It was observed that at a high TMAH concentration, the particle size significantly approached the crystallite size, which means the nanocrystalline powder is being changed into single crystal powder. Titanium isopropoxide was converted into hexahydroxo titanate ($Ti(OH)_6^{2-}$) by reaction with water and OH^- ions. The formed $Ti(OH)_6^{2-}$ reacted with Ba^{2+} ions dispersed in the solution for the crystallization of perovskite $BaTiO_3$ [38]. Therefore, if TMAH concentration (OH^- concentration) is high, the formation rate of negatively charged $Ti(OH)_6^{2-}$ becomes high. This results in a high concentration of $Ti(OH)_6^{2-}$ in the solution before reacting with [Ba^{2+}] ions. High concentration of $Ti(OH)_6^{2-}$ enhances the rate of nucleation, resulting in the lower crystallite and particle size. The SEM micrograph in Fig. 2.6 shows the morphology of the powder processed at high TMAH concentration (1.46M). Nearly spherical shape and less agglomeration were seen and the average particle size was slightly larger than one calculated from S_{bet}.

Fig. 2.7 shows increased entrapped or adsorbed OH^- content with increasing TMAH concentration, but it became almost constant above 1.25M of TMAH concentration. The a-axis was highly enlarged from 0.4015 to 0.4039nm corresponding to an increase in OH^- concentration in the solution. Therefore, these data indicate that the higher OH^- concentration in the solution accelerates the crystallization speed to the formation of smaller particles. At the same time, more OH^- ions are entrapped into the lattices as expected, which cannot be a suitable condition to prepare tetragonal phase $BaTiO_3$ in this WACS process.

According to Fig. 2.8, the obtained result of dielectric properties was quite similar to the one shown in Fig. 2.4 for the [Ba^{2+}] effect. The dielectric constants of the powders were not affected by TMAH concentration, even though the particle size, the a-axis, and OH^- content were widely varied with TMAH concentration. This should be because of the narrow range of tetragonality change, which is the same reason mentioned in the [Ba^{2+}] effect. In fact, the tetragonality and dielectric constant are expected to be influenced by the concentration of lattice OH^-, but it was observed that both properties, for all nano-particles synthesized here and in the [Ba^{2+}] effect, are little affected with the lattice OH^- content. In order to explain this, it can be assumed that the dielectric constant of nano-size powder which contains more than a certain amount of lattice OH^- is little changed with further lattice OH^- content because the tetragonal phase in a powder is also little changed above the same content of lattice OH^-.

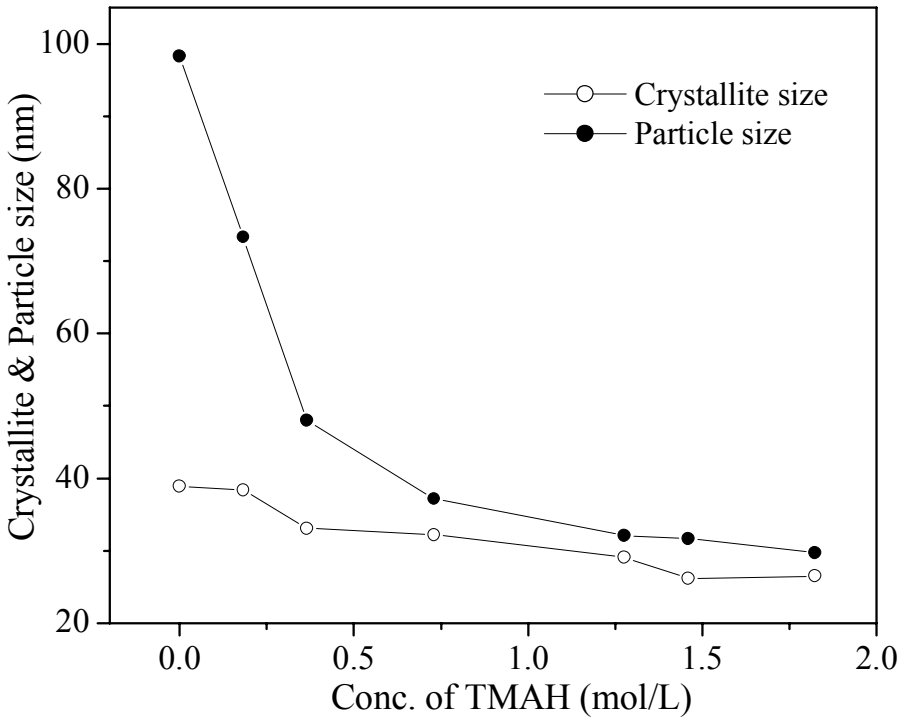

Figure 2.5 Crystallite and particle size of $BaTiO_3$ powders synthesized by different values of the TMAH concentration in the starting solution from 0 to 1.46M

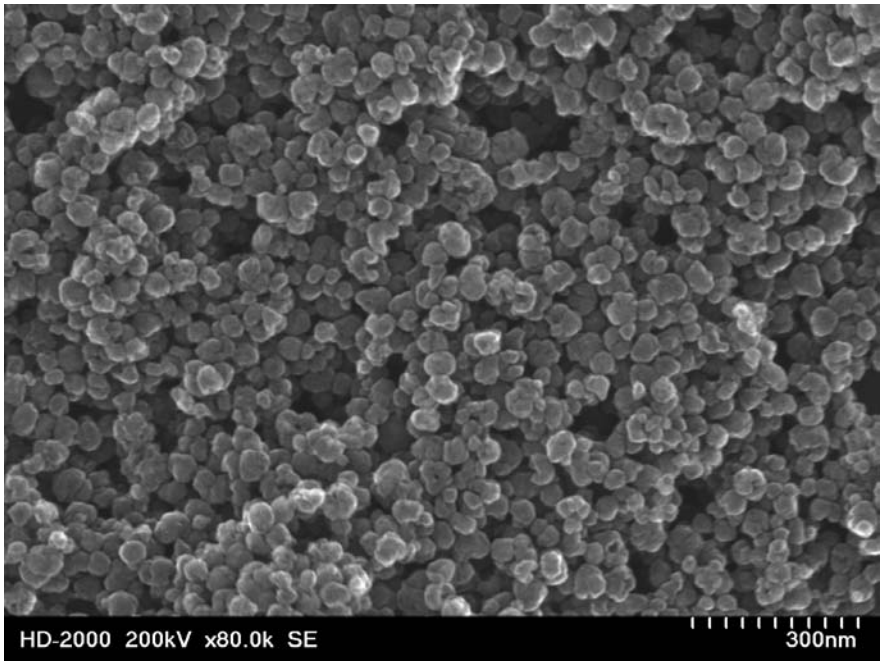

Figure 2.6 SEM micrograph of the $BaTiO_3$ powder synthesized at 1.46M of TMAH concentration

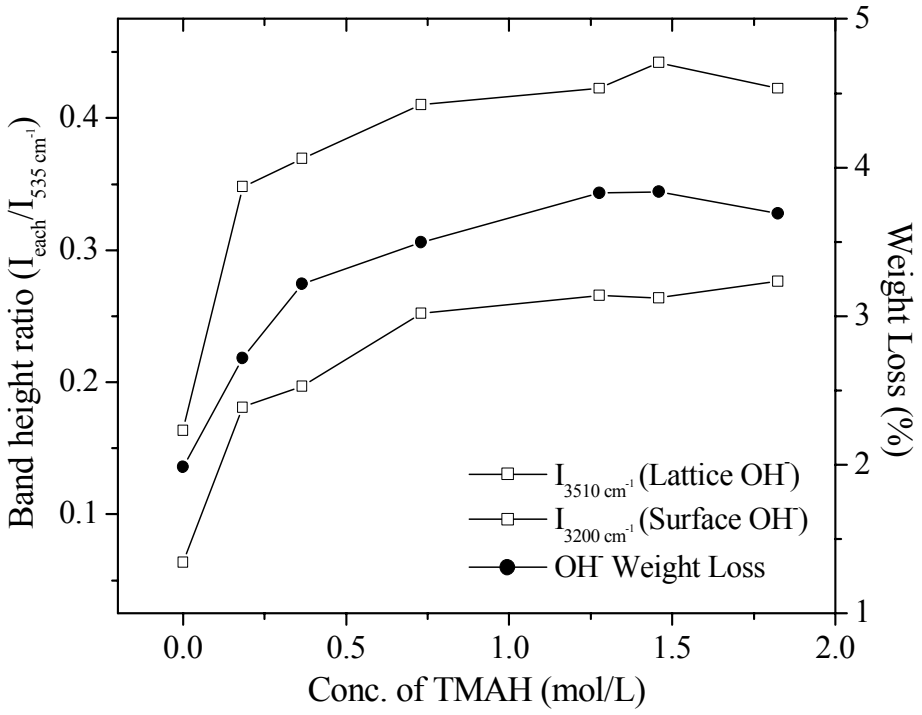

Figure 2.7 Normalized band height ratios of lattice and surface OH^- groups and weight loss of OH^- groups between 100 and 700 ^oC as a function of TMAH conc.

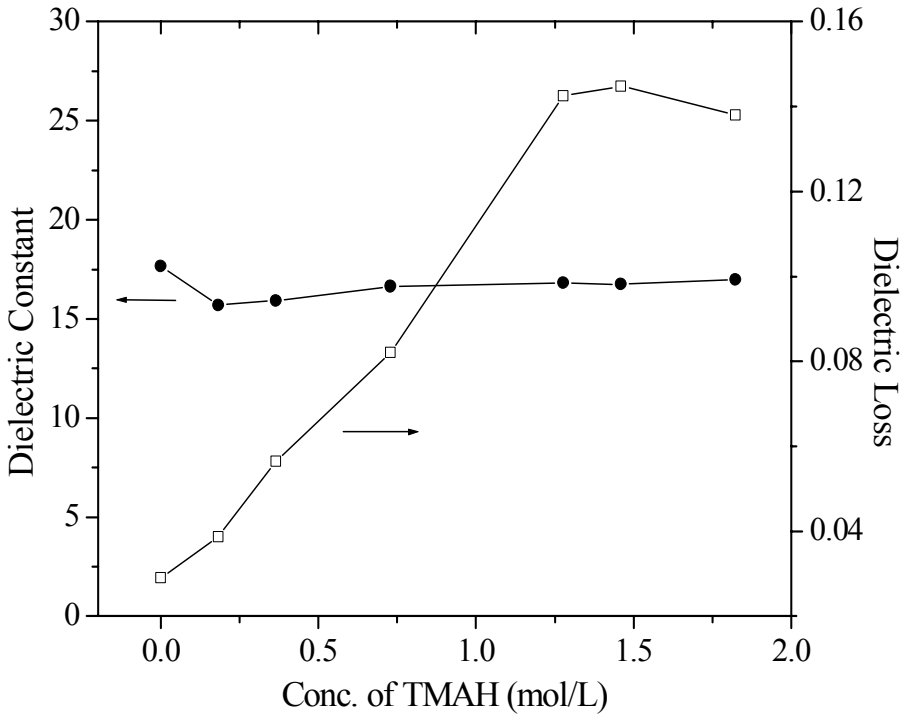

Figure 2.8 Room temperature dielectric constant and loss of castor oil-matrix composite with 30vol% of $BaTiO_3$ powder as a function of TMAH concentration

3.3. Effect of reaction time

The results in this section were obtained from $BaTiO_3$ powders synthesized for a reaction time ranging from 4 to 24 hrs in the solution containing [Ba^{2+}] of 0.2M without TMAH. Fig. 2.9 shows the SEM micrographs of $BaTiO_3$ powder synthesized at different reaction times of 4, 14, and 24 hrs. The homogeneously dispersed $BaTiO_3$ powder with a nearly spherical shape was seen in Fig. 2.9(a). However, with increasing reaction time, the shape of the powders changed from spherical particles to polygonal particles with a porous morphology, which should be formed by the aggregation of smaller particles. Consequently, the particle size increased to around 350 nm.

Fig. 2.10 shows that OH^- group content slowly decreased with increasing reaction time. The reduced amount of OH^- groups was relatively small, but the a-axis of unit lattice highly shrank from 0.4015 to 0.3990nm. It is observed that the FWAH values of the peak (200) gradually increased with longer reaction time. Considering the increase in particle size and high shrinkage in a-axis down to 0.3990nm, this increase in the FWAH should be due to the recovery of tetragonality in the powder rather than decrease in crystallite size [39]. Under this hypothesis, the c/a ratio was calculated, and it was increased from 1.0018 to 1.0040 with reaction time.

Fig. 2.11 shows that the dielectric constant also increased with reaction time. This result should indicate that the dielectric constant was enhanced with this conversion from cubic to tetragonal phase. This corresponds to the claim mentioned above that the dielectric constant is dependent on the tetragonality of the powder. Using all the

synthesized samples, including ones prepared in high [Ba^{2+}] and TMAH concentration, the effect of lattice OH^- concentration on both the tetragonality and dielectric constant was investigated. Lattice OH^- content was estimated by calculating weight loss caused by calcination with TGA between 400 and 700 ^oC. According to Fig. 2.12, the behavior of both tetragonality and the dielectric constant with lattice OH^- concentration was quite similar. Above an OH^- concentration of around 0.35 wt%, the dielectric constant and tetragonality was almost kept constant, but below around 0.35 wt% both of them were increased. This result agreed with the assumption mentioned above that the tetragonality and dielectric constant are little changed with lattice OH^- concentration when the lattice OH^- content in a powder is more than a certain amount of lattice OH^-. Regarding the dielectric loss, it was slightly decreased, corresponding to the small reduction of OH^- groups as shown in Fig. 2.10.

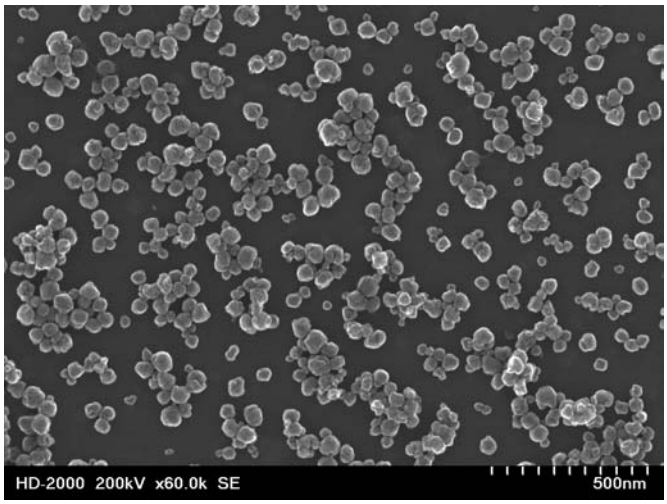

(a)

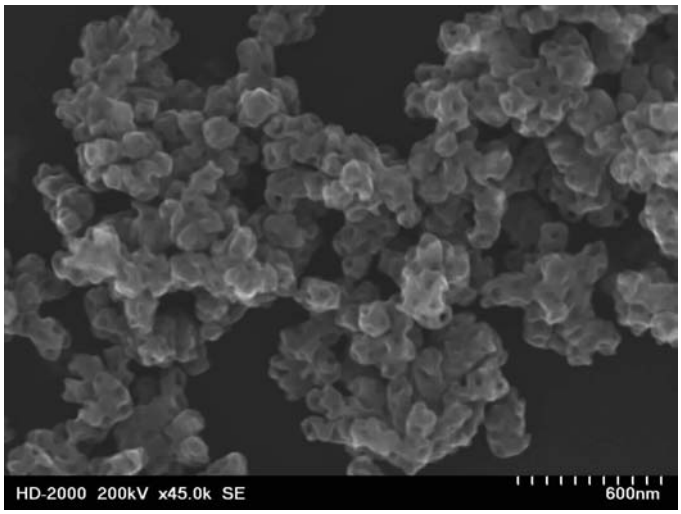

(b)

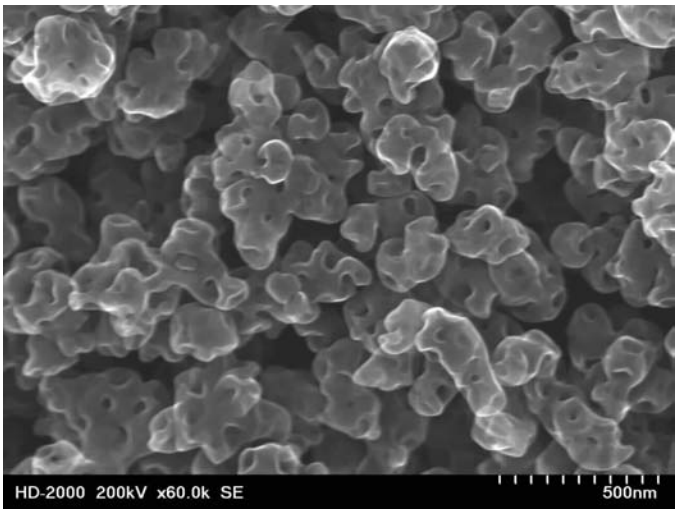

(c)

Figure 2.9 SEM micrograph of the $BaTiO_3$ powder synthesized at different reaction time (a)4hrs, (b)14hrs, (c)24hrs

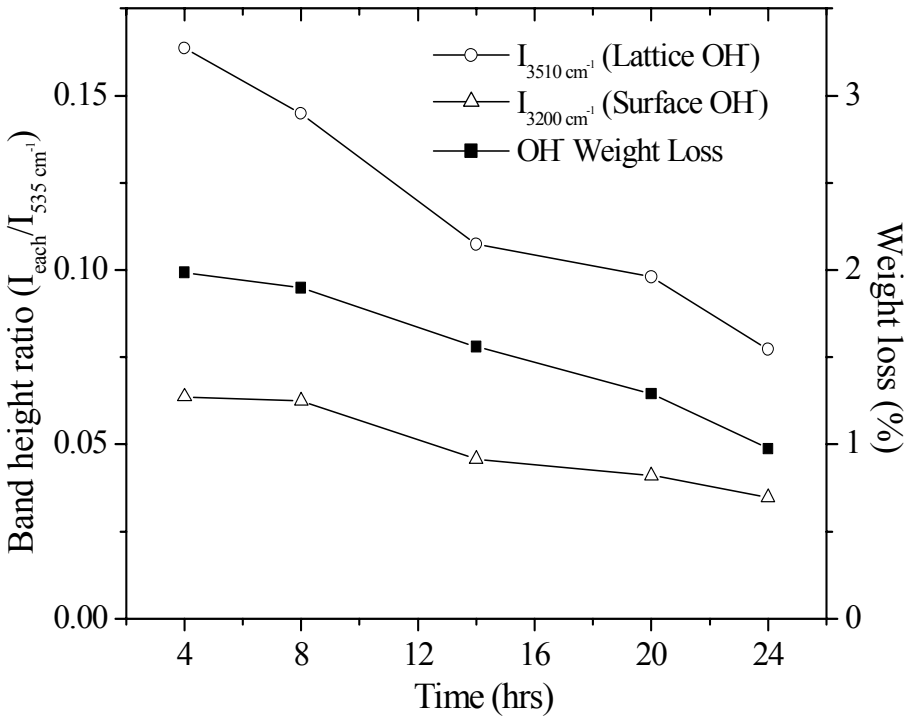

Figure 2.10 Normalized band height ratios of lattice and surface OH^- groups and weight loss of OH^- groups between 100 and 700 ^oC as a function of reaction time

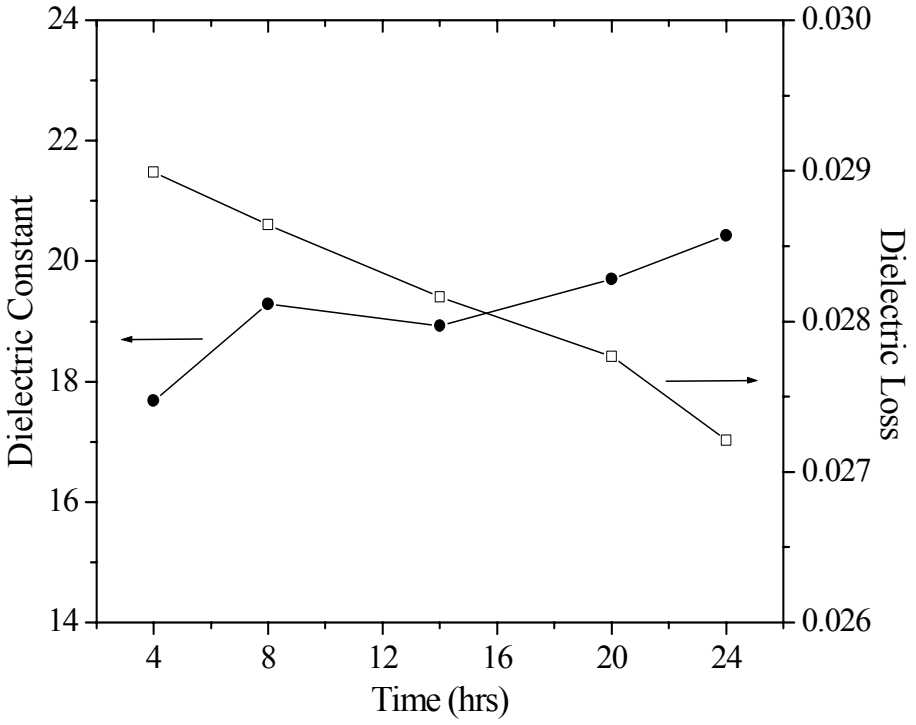

Figure 2.11 Room temperature dielectric constant and loss of castor oil-matrix composite with 30vol% of $BaTiO_3$ powder as a function of reaction time

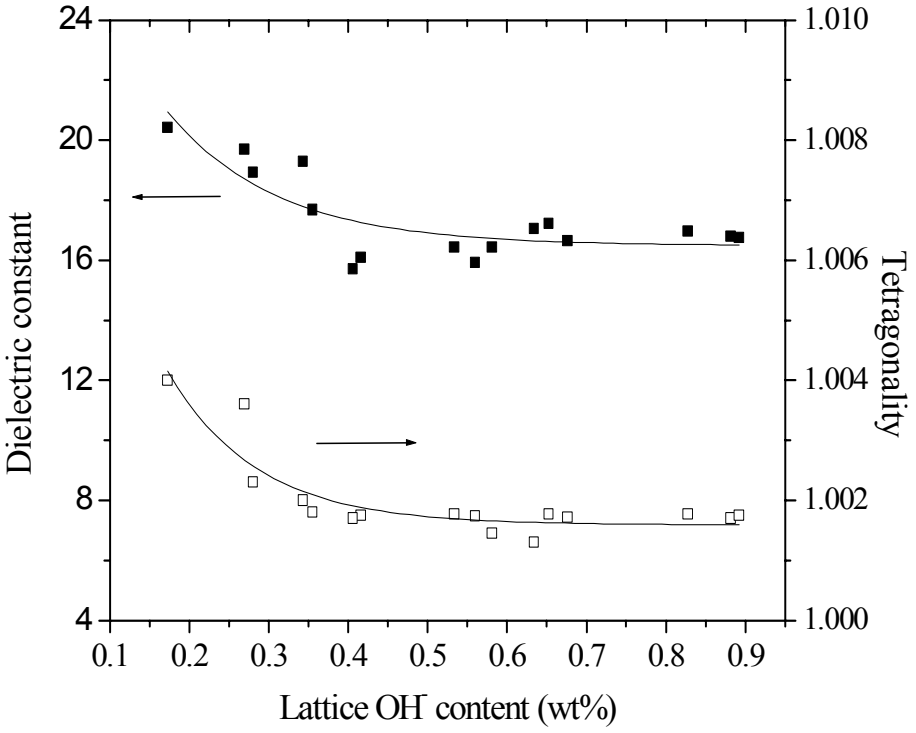

Figure 2.12 Dielectric constant and tetragonality as a function of lattice OH^- content

3.4. Effect of heat treatment

To investigate the effects of heat treatment on the $BaTiO_3$ nanopowder with high OH^- content, the powder synthesized with high TMAH concentration of 1.46M was used. This powder is the same as the one shown in Fig. 2.6. As heat treatment was performed under mild calcination temperature between 200 and 700 ^oC for 4 hrs, the change in particle size of the starting powder should be limited and small [32]. Fig. 2.13 shows that when the calcination temperature is increased, the band height ratio of both OH^- groups were highly decreased, which means that OH^- groups are desorbed from the powder by the heat treatment. As a result, the a-axis shrank from 0.4028 to 0.4004nm. However, the XRD data showed that the crystal phase remained cubic for all calcined samples even after heat treatment at 700 ^oC and the FWAH values of the peak (200) did not increase. It is thus not seen that the tetragonality is increased with calcinations temperature despite the disappearance of a large amount of the lattice OH^- defects. This should be because there still exists the lattice strain associated with the presence of remaining lattice OH^- defects and cationic vacancies [10]. Regarding crystallite size, Fig. 2.14 indicates that between 0 and 200^oC and between 600 and 700^oC, there was a small increase in crystallite size, but over the wide range from 200 to 600^oC, the crystallite size remained constant. In contrast, the specific surface area was significantly reduced with increasing calcination temperature. This should be mainly associated with a decrease in the size and number of pores existing in $BaTiO_3$ powders rather than desorption of OH^- groups from the powder. According to Fig. 2.15, the dielectric constant is highly improved with

increasing temperature, and eventually, the dielectric constant of the powder calcined at 700 ^{o}C became about twice as large as that of a non-heat-treated sample. Considering that the reduction of OH^- defects with heat treatment did not contribute to an increase in tetragonality and another major property change with heat treatment was seen in only values of specific surface area, it can be concluded that the biggest contribution to the enhancement for dielectric constant should be the decrease in the specific surface area which is equal to the decrease in the size and number of pores existing within the powder. The dielectric loss decreased with high calcination temperature as the OH^- groups were removed with heat treatment.

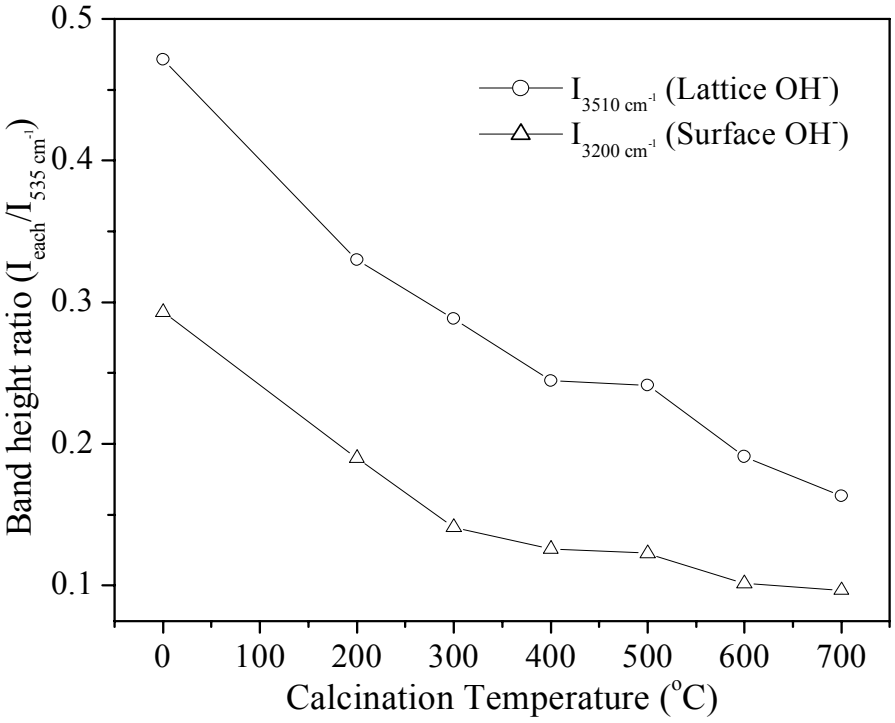

Figure 2.13 Normalized band height ratios of lattice and surface OH^- groups as a function of calcination temperature between 0 and 700 ^oC

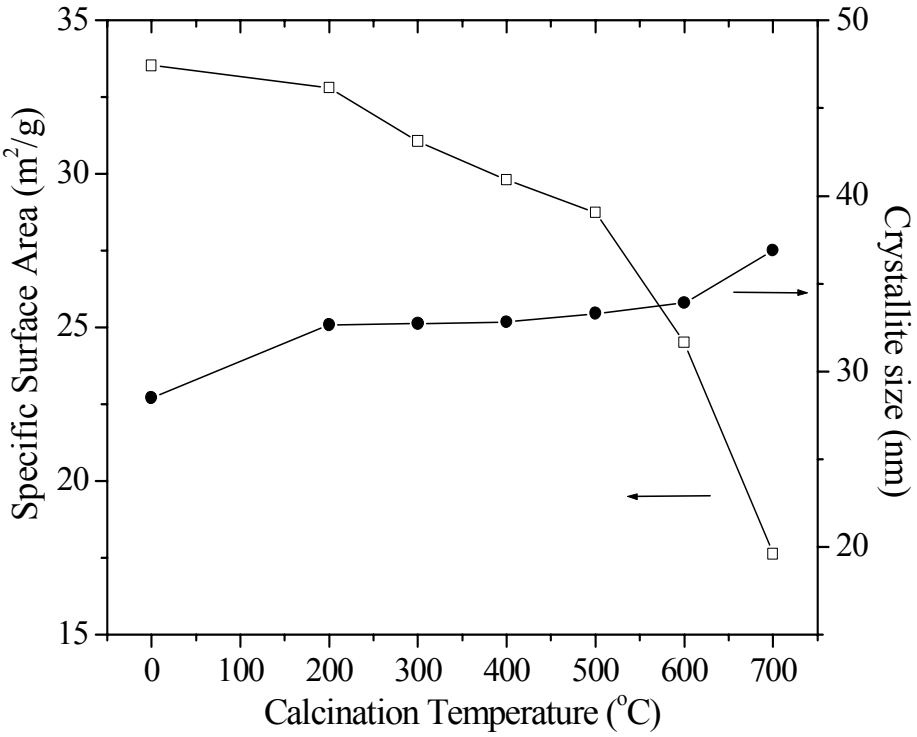

Figure 2.14 Specific surface area and crystallite size as a function of calcination temperature between 0 and 700 °C

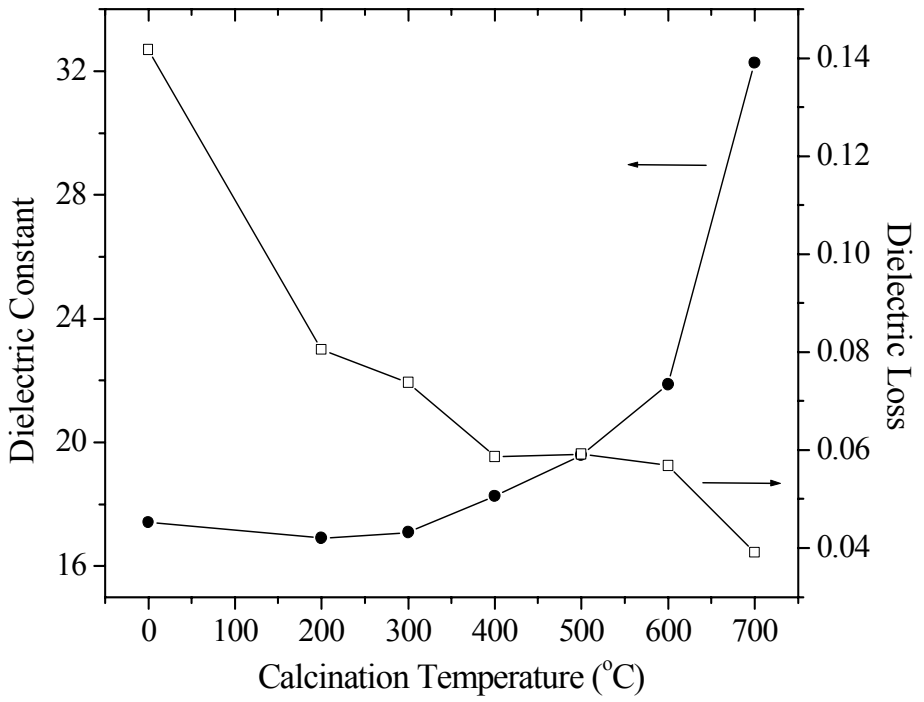

Figure 2.15 Room temperature dielectric constant and loss of castor oil-matrix composite with 30vol% of $BaTiO_3$ powder as a function of calcination temperature between 0 and 700 °C

4. Conclusions

$BaTiO_3$ nano-powders have been successfully synthesized with WACS process under mild conditions. The particle and crystallite size and content of OH^- groups in the powder were highly varied by changing the values of processing parameters such as $[Ba^{2+}]$ and TMAH concentration. Higher $[Ba^{2+}]$ and TMAH concentrations led to smaller crystallite and particle size and higher concentration of OH^- groups in the powder. The dielectric constant changed little with $[Ba^{2+}]$ and TMAH concentration while the dielectric loss increased with increasing concentration of the OH^- groups. The longer reaction time significantly changed the morphology of the powder and formed larger particles due to the aggregation of small particles. The OH^- content in the powder decreased with longer reaction time. As a result, the tetragonality of the powder was recovered with the longer reaction time, which increased the dielectric constant. The dielectric constant was dependent on the tetragonality in the powder. The dielectric constant and tetragonality are increased below lattice OH^- concentration of around 0.35 wt%, and above this concentration, both of them are almost kept constant. Heat treatment highly improved the dielectric properties, which should be related to the elimination of the pores and to the desorption of OH^- groups from the powder.

Reference

1. C. Pithan, D. Hennings and R. Waser, Int. J. Appl. Ceram. Technol. **2** [1] 1 (2005)

2. Y. Rao and C.P. Wong, J. Appl. Polym. Sci. **92** 2228 (2004)

3. Y. Bai, Z.Y. Cheng, V. Bharti, H.S. Xu and Q.M. Zhang, Appl. Phys. Lett. **76** 3804 (2000)

4. S. Bhattacharya and R.R. Tummala, J. Electron. Packag. **124** 1 (2002)

5. N.G. Devaraju, E.S. Kim and B.I. Lee, Microelectro. Engin. **82** 71 (2005)

6. L. Qi, B.I. Lee, W.D. Samuels, G.J. Exarhos and S.G. Parler, Jr., J. Appl. Polym. Sci. **102** 967 (2006)

7. P.K. Dutta and J.R. Gregg, Chem. Mater. **4** 843 (1992)

8. S. Wada, H. Chikamori, T. Noma and T. Suzuki, J. Mater. Sci. Lett. **19** 245 (2000)

9. J. Moon, E. Suvaci, T. Li, S.A. Sostantino and J. H. Adair, J. Eur. Ceram. Soc. **22** 809 (2002)

10. R. Vivekanandan and T.R.N. Kutty, Power Technol. **57** 181 (1989)

11. S. Lu, B.I. Lee, Z, L, Wang and W.D. Samuels, J. Crys. Growth **219** 269 (2000)

12. H. Xu, L. Gao and J. Guo, J. Eur. Ceram. Soc. **22** 1163 (2002)

13. H. Xu and L. Gao, J. Am. Ceram. Soc. **86** 1 203 (2002)

14. D.F.K. Hennings, C. Metzmacher and B.S. Schreinemacher, J. Am. Ceram. Soc. **84** [1] 179 (2001)

15. T. Noma, S. Wada, M. Yano and T. Suzuki, J. Appl. Phys. **80** 9 (1996)

16. D. Hennings and S. Schreinemacher, J. Eur. Ceram. Soc. **9** 41 (1992)

17. I. J. Clark, T. Takeuchi, N. Ohtori and D. Sinclair, J. Mater. Chem. **9** 83 (1999)

18. X. Wang, B.I. Lee, M.Z. Hu, E.A. Payzant and D.A. Blom, J. Mater. Sci. Lett. **22** 557 (2003)

19. X. Wang, B.I. Lee, M.Z. Hu, E.A. Payzant and D.A. Blom, J. Mater. Sci. – Mater. Electron. **14** 495 (2003)

20. X. Wang, B.I. Lee, M. Hu, E.A. Payzant and D.A. Blom, J. Euro. Ceram. Sci. **26** 2319 (2006)

21. N.G. Devaraju, B.I. Lee, M. Viviani, P. Nanni and E.S. Kim, J. Mater. Sci. **41** 3335 (2006)

22. B.I. Lee, X. Wang, S.J. Kwon, H. Maie, R. Kota and J. H. Hwang, J. G.. Park, M. Hu, Microelectron. Eng. **83** 463 (2006)

23. R. Kota, A.F. Ali and B.I. Lee, M.M. Sychov, Microelectron. Eng. (in press)

24. A. Testino, M.T. Buscaglia, M. Viviani, V. Buscaglia and P. Nanni, J. Am. Ceram. Soc. **87** [1] 79 (2004)

25. A. Testino, V. Buscaglia, M.T. Buscaglia, M. Viviani and P. Nanni, Chem. Mater. **17** 5346 (2005)

26. M. Viviani, M.T. Buscaglia, A. Testino, V. Buscaglia, P. Bowen and P. Nanni, J. Euro. Ceram. Soc. **23** 1383 (2003)

27. D.R. Brezinski, An Infrared Spectroscopy Atlas for the Coatings Industry, 4th ed., Blue Bell, 1991, Vol. 1

28. S.W. Lu, B.I. Lee, Z.L. Wang and W.D. Samuels, J. Crystal Growth **219** 269 (2000)

29. S.W. Lu, B.I. Lee and L.A. Mann, Materials Letters, **43** 102 (2000)

30. B.I. Lee, J. Electroceram. **3** [1] 53 (1999)

31. S.K. Patil, N. Shah, F.D. Blum and M.N. Rahaman, J. Mater. Res. **20** 12 (2005)

32. T. Noma, S. Wada, M. Yano and T. Suzuki, J. Appl. Phys. **80** 9 5223 (1996)

33. S. Wada, T. Suzuki and T. Noma, J. Ceram Soc, Jpn. **103** 1220 (1995)

34. S. Wada, H. Yasuno, T. Hoshina, Song-Min Nam, H. Kakemoto and T. Tsurumi, Jpn. J. Appl. Phys. **42** 6188 (2003)

35. S. Wada, M. Narahara, T. Hoshina, H. Kakemoto and T. Tsurumi, J. Mate. Sci. **38** 2655 (2003)

36. G. Busca, V. Buscaglia, M. Leoni and P. Nanni, Chem. Mater. **6** 955 (1994)

37. S.G. Kwon, B.H. Park, K. Choi, E.S. Choi, S. Nam, J. W. Kim and J. H. Kim, J. Euro. Ceram. Soc. **26** 1401 (2006)

38. S. Yoon, S. Baik, M.G. Kim and N. Shin, J. Am. Ceram. Soc. **89** 6 1816 (2006)

39. E. Ciftci, M.N. Rahaman and M. Shumsky, J. Mate. Sci. **36** 4875 (2001)

CHAPTER 3

SYNTHESIS AND CHARACTERIZATION OF BARIUM TITANATE NANO-POWDER SYNTHESIZED BY SOLVENT-BASED AMBIENT CONDITION SOL PROCESS

Abstract

Nanocrystalline barium titanate, $BaTiO_3$, powders have been successfully synthesized via solvent-based ambient condition sol (SACS) process, using barium hydroxide and titanium isopropoxide. The effects of an organic solvent concentration in the aqueous solution on the properties of the powder were investigated with XRD, TEM, and FTIR. Two different solvents, such as 2-propanol and t-butyl alcohol, were used as organic solvents. The crystal phase of as-prepared $BaTiO_3$ was cubic structure at room temperature. The particle size and crystallite size decreased with higher solvent concentration. The smallest crystallite and particle sizes were obtained from a water-free organic solvent. Nearly spherical and well-dispersed $BaTiO_3$ nanoparticles with narrow particle size distribution were obtained according to SEM micrographs. The contents of OH^- groups in the powder continuously increased until around 50~60vol% of organic solvent. Above this, OH^- contents started to decrease. The change in a-axis in perovskite lattice approximately agreed with the OH^- content data. At high solvent compositions of around 70-80vol%, the lattice OH^- content and a-axis were recorded as the lowest value, leading to superior dielectric properties.

1. Introduction

Since an increase in tetragonal phase in $BaTiO_3$ leads to the enhancement of dielectric properties, higher tetragonality should be desirable for the applications of MLCC and embedded capacitors. If the incorporation of OH^- ions is successfully prevented during a synthesis process, the lattice strain is removed from the perovskite lattice, resulting in an increase in the tetragonality of the powder or the formation of complete tetragonal phase.

The primary reason for this incorporation of OH^- groups in the lattice in a hydrothermal process should be that this process uses a lot of water to dissolve the starting precursors and a high alkaline solution to obtain high pH. Thus, a lot of hydroxyl species exist in the solution and they are inevitably incorporated into $BaTiO_3$ lattices. To overcome this problem, preparing $BaTiO_3$ in a mixture of organic solvent and water, or totally water-free organic solvent, may be a promising way to reduce or even eliminate the OH^- defects in as-prepared $BaTiO_3$ powder. As mentioned in the former chapter, Kwon et al. [1] reported that a mixture solution of ethanol and water with no additional OH^- ions (in particular, 40-80vol% of ethanol in mixed solvent) can successfully produce the fine $BaTiO_3$ powders with high tetragonality at 210 ^oC in an autoclave. This should imply that the fewer amount of OH^- ions in the starting solution, which is obtained by increasing organic solvent composition, is effective for synthesis of high tetragonality $BaTiO_3$. Thus, controlling the concentration of OH^- ions in the reaction medium can be important to synthesize tetragonal phase $BaTiO_3$ fine powder.

In this study, $BaTiO_3$ nanopowders were prepared in a mixed solvent of alcohol and water under nearly ambient conditions, using barium hydroxide octahydrate and titanium isopropoxide. By changing the concentration of organic solvent in the mixed solvent, the availability of OH^- ions was varied. It was investigated how the properties of the powder changed with the solvent composition in the mixed solvent.

2. Experimental

2.1. Powder synthesis

$BaTiO_3$ powder was directly synthesized by a precipitation process in a mixture solution of water and organic solvent under low temperature in a sealed Teflon jar. Barium hydroxide (Chemical Products Corporation, Cartersville, GA) and titanium isopropoxide (Tyzor TPT, Dupont chemical solutions enterprise, Wilmington, DE) were used as the starting materials. Two different kinds of organic solvents are individually used as reaction media, 2-propanol (Alfa Aesar, 99.5%) and t-butyl alcohol (Fisher, 99.5%). Barium hydroxide was dissolved in a mixture solution of distilled water and an organic solvent at room temperature by stirring in 500ml Teflon jar to form solution A. Solution B was formed by dissolving titanium isopropoxide in an organic solvent by stirring. Solution B was slowly added to solution A with constant stirring. The Ba^{2+} ion concentration ($[Ba^{2+}]$) and Ba/Ti precursor ratio in the mixture solution was kept constant at 0.2M and 1.3, respectively. The resulting white slurry contained in the Teflon jar was then heated to 120 ^oC for 6 hours in an oil bath. In order to get rid of barium carbonates

and extra barium ions, the product solids were washed twice with a diluted acetic acid solution and distilled water, respectively. These solids were dried overnight at 80 ^{o}C in a vacuum.

To study the effects of a change in dissociation of titanium isopropoxide in the solution, TMAH (25% w/w aq. soln. Alfa Aesar) was used as the base. The results were discussed in the only 3.31 section. TMAH was slowly added into Ba and Ti mixed solvent with vigorous stirring before heating and the TMAH concentration was maintained at 0.37M. The [Ba^{2+}] and Ba/Ti precursor ratio in the mixture solution was kept constant at 0.2M and 1.3, respectively.

2.2. Powder characterization

The as-prepared powders were examined by XRD. Room temperature XRD patterns of $BaTiO_3$ were recorded in the 2θ range of 20^o - 80^o and 37^o - 40^o (RTXRD, Scintag PADV using CuKa with λ=0.15406 nm). The crystallite size of $BaTiO_3$ was calculated from the (110) peak of the corresponding XRD pattern using Scherrer equation, $D=0.9\lambda/\beta\cos\theta$, where λ is the wavelength, θ is the angle of diffraction, and β is the FWHM. The a-axis was also calculated using the (110) peak of XRD. The value of the a-axis was dependent on the position of the peak, which was shifted by changing the solvent composition. The particle size and the morphology of $BaTiO_3$ powders were investigated by a TEM (Hitachi, HD2000). To evaluate the OH^- group content in the

powders, a fourier transform infrared spectrometer (FT-IR) (Nicolet Magna-IR 550) was used.

The dielectric constants of the powders were characterized by measuring the capacitance of the particle composites. A capacitor was fabricated using a procedure described elsewhere [2, 3], using a castor oil as the matrix with 30 vol% of powder in the slurry paste form, which filled the Teflon-cell with aluminum plate electrodes. Capacitance was measured at 1 MHz using an LCR meter (HP 4284A Precision LCR Meter). The dielectric constant values (K) of the capacitors were calculated from the measured capacitance data using the equation: [$C= K\varepsilon_o A/t$], where ε_o is the dielectric permittivity of the free space, ($8.854*10^{-12}$ F/m), A is the contact area between the electrode and composite paste ($1cm^2$), and t is the thickness of the ceramic specimen, (0.4 cm).

3. Results and Discussion

3.1. Crystal structure and crystallite size

Table 1 shows the physical properties of the solvents used in preparation of the nanocrystalline $BaTiO_3$ powders. The concentration of organic solvents used in the starting solution was varied from 5 to 100%. By changing the composition of the organic solvents in the mixture, the concentration of OH^- available for the reaction was varied. A higher organic solvent composition provides the condition of less OH^- ions in the starting solution. Fig. 3.1 shows the room temperature XRD patterns of the $BaTiO_3$ powders as a

function of isopropanol concentration. The crystal structure of $BaTiO_3$ was assigned to the cubic phase for all prepared samples including ones synthesized with butanol as the peaks for tetragonal phase were not seen with XRD. It is observed that as the composition of organic solvent was increased, the peak intensities decreased while the values of FWAH increased. This implies that the formed nanocrystals tend to become smaller when solvent composition increases. The XRD patterns of $BaTiO_3$ prepared with butanol also showed the same trend.

Fig. 3.2 shows that the crystallite size decreased with increasing organic solvent concentration. This behavior should be associated with a decrease in medium polarity with higher solvent content, leading to a change in solubility of $BaTiO_3$ in the mixed solvent. This will be discussed in the later section.

Table 1 The physical properties of the organic solvents used for synthesis

Organic Solvent	Mol. wt (g/mol)	Boiling point (°C)	Density (g/cm^3)	Dielectric constant
2-propanol	88.15	82.2	0.786	18.3
Butanol	74.12	82.4	0.785	12.5

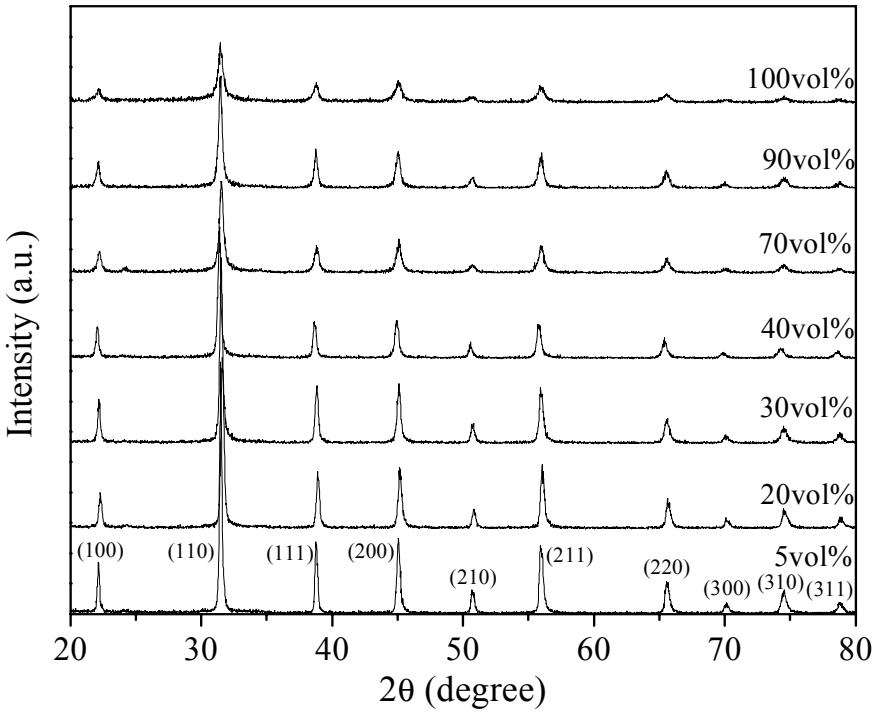

Figure 3.1 XRD patterns of $BaTiO_3$ powders synthesized by isopropanol as a function of the organic solvent composition

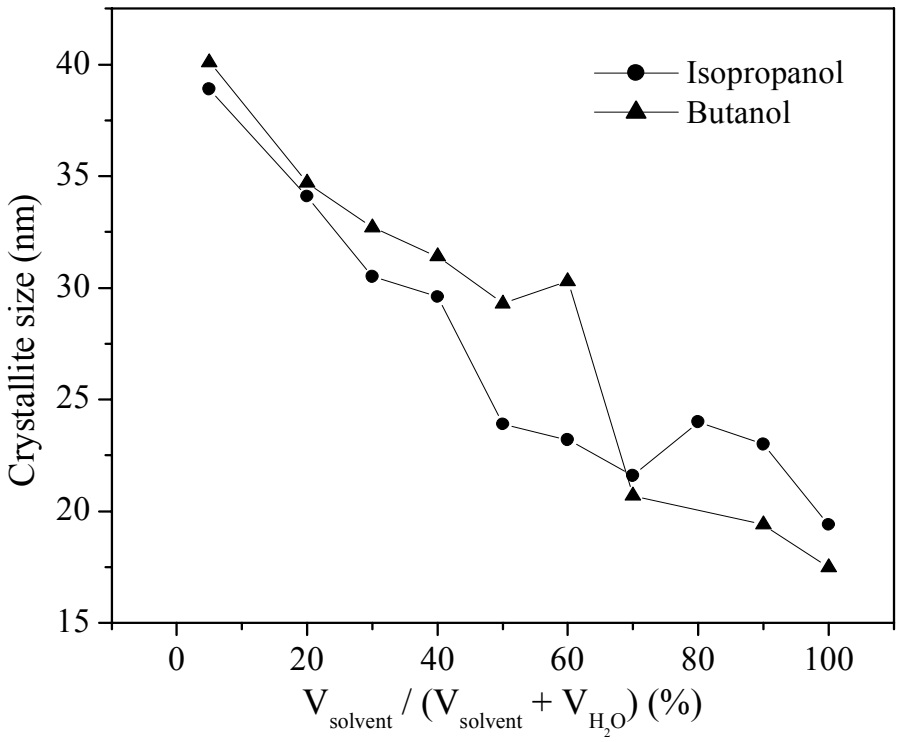

Figure 3.2 Crystallite size of $BaTiO_3$ powders synthesized by isopropanol and butanol as a function of the organic solvent composition

3.2. Morphology, particle size and particle formation

Fig. 3.3 shows the SEM micrographs of $BaTiO_3$ powder synthesized with isopropanol and butanol at different solvent compositions. The homogeneously dispersed $BaTiO_3$ particles with a nearly spherical shape were seen in Fig. 3. It was observed that the particle size is decreased with higher organic solvent compositions in the same way the crystallite size is decreased in Fig. 3.2.

The formation process of the $BaTiO_3$ particles involves a reaction between the Ba^{2+} ions in the solution and the hexahydroxy titania species ($Ti(OH)_6^{2-}$). The titanium

hexahydroxides are formed by a reaction of titanium isopropoxide with water and OH^- ions. Then the tiny $BaTiO_3$ nucleates and grows to become crystallites followed by aggregation of the as-prepared crystallites or secondary nucleation such as heterogeneous nucleation at the surface of $BaTiO_3$ crystallites created by the former nucleation. This will lead to the formation of the final nanocrystalline $BaTiO_3$ powders as shown in eq. (1) below, beginning from $Ti(OR)_4$ as titanium isopropoxide [4].

$$\begin{aligned} & Ti(OR)_4 + 4H_2O + Ba^{2+} + 2(OH)^- \\ & \rightarrow Ti(OH)_6^{2-} + Ba^{2+} + 4ROH \\ & \rightarrow BaTiO_3 + 4ROH + 3H_2O \end{aligned} \qquad (1)$$

The sizes of the particles that precipitate out of the solution depends, in general, on the relative rates of nucleation and crystallite growth [5-10], which are controlled by changing the synthesis conditions such as the reactant concentration, the pH, the Ba/Ti ratio of reactant precursors, and temperature. If the nucleation rate is high, the large number of small crystallites is quickly formed. In addition, the aggregation process of the as-prepared crystallites and secondary nucleation tend to be suppressed as the rate increased. As a result, a large number of the particles with small particle and crystallite size are produced at the high rate of nucleation.

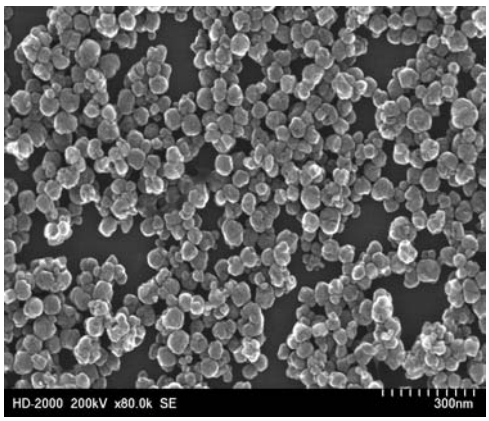

(a) Isopropanol 5vol%

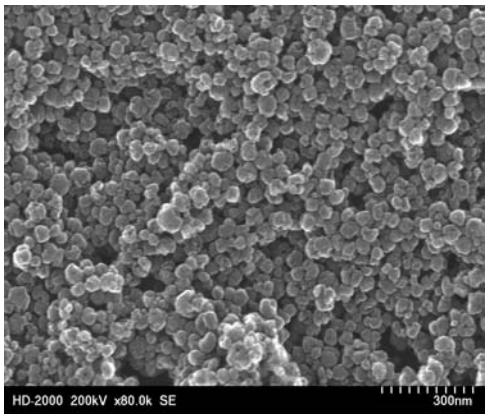

(b) Isopropanol 20vol%

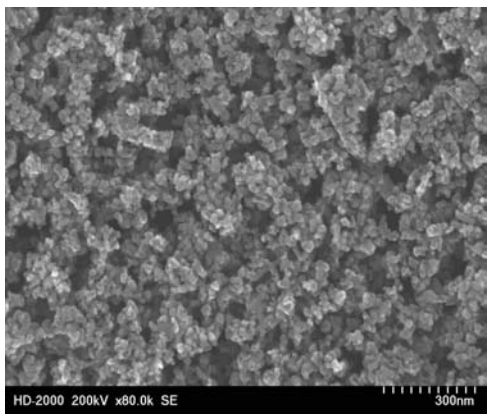

(c) Isopropanol 100vol%

Figure 3.3 SEM micrographs of the $BaTiO_3$ powders synthesized by isopropanol at the solvent composition of (a) 5vol%, (b) 20vol%, and (c) 100vol%

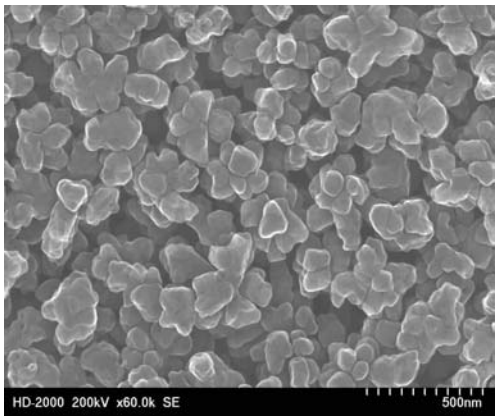

(d) Butanol 5vol%

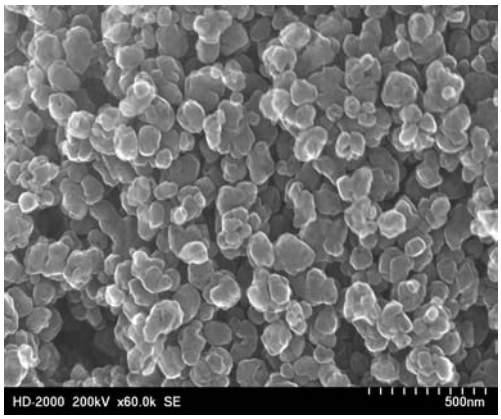

(e) Butanol 20vol%

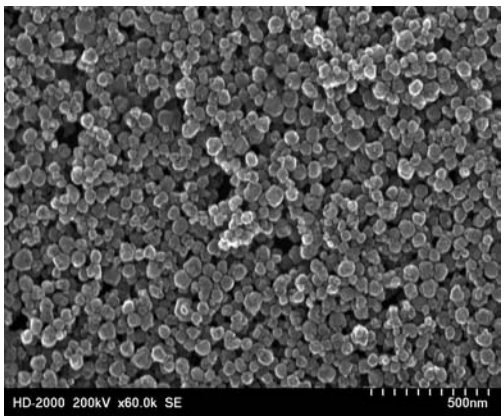

(f) Butanol 100vol%

Figure 3.3 SEM micrographs of the $BaTiO_3$ powders synthesized by butanol at the solvent composition of (d) 5vol%, (e) 20vol%, and (f) 100vol%

3.3. Effects on crystallite size and nucleation

3.3.1 Effect of change in dissociation of Ti isopropoxide

It is reported that with higher starting reactant concentrations, such as that of Ba and Ti species in the solution, the rate of nucleation becomes higher [5-8]. This implies that the solubility or dissociation of the starting precursors in the mixed solvent also affects the rates of nucleation and crystal growth. Thus, higher solubility or dissociation of the reactants should result in a higher rate of nucleation and smaller crystallite size. In order to prove this, the effect of the addition of base (TMAH) into a mixed solvent with different isopropanol content on the crystallite size was investigated. According to Table 2, the sizes of all samples synthesized by isopropanol with base were smaller than those synthesized only by isopropanol, regardless of isopropanol content in a mixed solvent. Since isopropanol with base has higher OH^- content, more titanium isopropoxide hydrolyzed, forming a larger number of $Ti(OH)_6^{2-}$ nuclei (i.e. higher solubility or dissociation of Ti isopropoxide). This resulted in a higher nucleation rate and smaller crystallite size.

3.3.2. Effects of polarity change with organic solvent amount in a mixed solvent

As the proportion of organic solvent in aqueous solution increases, the polarity of the mixture solution decreases because of the lower dielectric constant of organic solvent. This decrease in the polarity of the medium leads to lowering the dissociation of starting precursors in the solution, causing the slower rates of nucleation. Therefore, it is expected

that by increasing the composition of organic solvent in aqueous solution, particles with larger crystallite and particle size are produced. However, this expectation conflicts with the experimental results as shown in Fig. 3.2 and Fig. 3.3. This incoherent phenomenon can be explained by considering the change in solubility and supersaturation of $BaTiO_3$ with the organic solvent composition. As mentioned in the previous chapter, nucleation rate is dependent on supersaturation [6,10]. Conventionally, the degree of supersaturation (S) is defined as the ratio of solute concentration (C) and saturation concentration (C_l) [10], i.e.

$$S = \frac{C}{C_l} \qquad (2)$$

where the subscript, "l" stands for liquid phase. Increasing the organic solvent composition in the solution, i.e., decreasing the polarity of the medium, leads to a decrease in the solubility of $BaTiO_3$. This is because increasing deviations in polarity between the medium and $BaTiO_3$ will increasingly reduce the solubility [11]. As a result, the supersaturation of $BaTiO_3$ is increased with higher organic solvent composition. This increased supersaturation condition leads to a higher rate of nucleation and smaller crystallite and particle size [5-7].

Compared to the effect of organic solvent nature on a crystallite size, the crystallite size of the samples synthesized with butanol became smaller at the large organic solvent compositions than that of the samples synthesized with isopropanol. It can be assumed

that, since butanol is less polar than isopropanol, it should have lower solubility of $BaTiO_3$. The resulting higher supersaturation leads to a smaller crystallite size.

3.4. OH^- defects

Fig. 3.4 shows the FT-IR adsorption spectra of $BaTiO_3$ powders synthesized with different amounts of butanol. As shown in Fig. 3.4, all the FT-IR data for the samples showed the broad band in the very wide wave number region from 2500 to 3700 cm^{-1}, which is caused by the O-H stretching vibration [12-17]. As mentioned earlier, this broad band is categorized into two main groups; lattice OH^- and surface-adsorbed OH^-. The sharp absorption band peak around 3510cm^{-1} in the broad region is assigned to O-H stretching vibration of lattice OH^- groups [13,16]. The strong peak seen around 535cm^{-1} is assigned to the band for the lattice vibrational mode of $BaTiO_3$ [17].

According to Fig. 3.4, at a high organic solvent composition, e.g., 90 and 100%, the broad band peak for OH^- groups becomes small and the lattice OH^- peak at 3510cm^{-1} tends to become unclear. Especially at the organic solvent composition of 100%, there was only broad band for surface OH^- and the sharp band peak for lattice OH^- was not observed. However, this cannot mean that the powder has no lattice OH^- defects in the unit lattices. Rather the feasible reason is that the broad surface OH^- band covered up the weaker band intensity of lattice OH^-. This should be because the particle size of powder synthesized at 100% solvent is quite small. The resulting surface areas become so large that the relatively larger amount of surface OH^- adsorbed on the powders. As a

consequence, it can be assumed that the lattice OH^- band was buried in the large surface OH^- broad band.

In order to relatively estimate the OH^- content in the as-prepared powders, semi-quantitative FT-IR analysis was performed by using the FT-IR baseline method and normalization [18-21]. The previous chapter work showed that the change in OH^- content estimated with this method corresponds well to the weight loss percent of OH^- measured with TGA. The broad band at $3200cm^{-1}$ was used to estimate the surface OH^- content. Measured OH^- band intensities of lattice and surface OH^- were normalized by the band intensity of $BaTiO_3$ at $535cm^{-1}$. As a result, the band height ratios of I_{3510}/I_{535} and I_{3200}/I_{535} were used to estimate the relative content of both lattice and surface OH^- in the $BaTiO_3$ particles. Fig. 3.5 (a) and (b) show the behavior of the normalized band ratios of the lattice and surface OH^- as function of isopropanol and butanol composition, respectively. It was observed that the contents of lattice OH^- and surface OH^- continued to increase until around 50~60vol%, but above 60vol%, they rapidly decreased until 80 or 90vol%. Eventually the relative contents of OH^- groups fall within almost the same level as that at lower organic solvent composition, but between 90 and 100vol%, a small increase in OH^- content was observed.

Table 2 The crystallite sizes of the samples synthesized with isopropanol with base or Isopropanol

Isopropanol amount in a mixed solvent (vol%)	Crystallite size (nm)	
	Without base	With base (TMAH 0.37 mol/L)
5	38.9	33.1
20	34.1	30.3
40	29.6	25.7
60	23.2	19.4

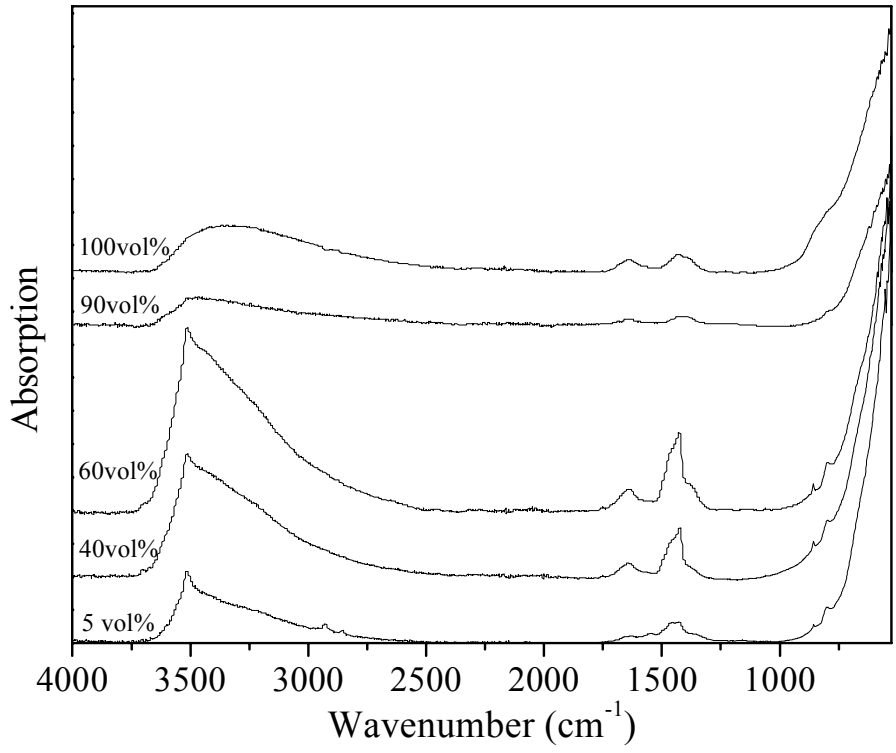

Figure 3.4 FT-IR absorption spectra of $BaTiO_3$ powders synthesized with different vol% of butanol

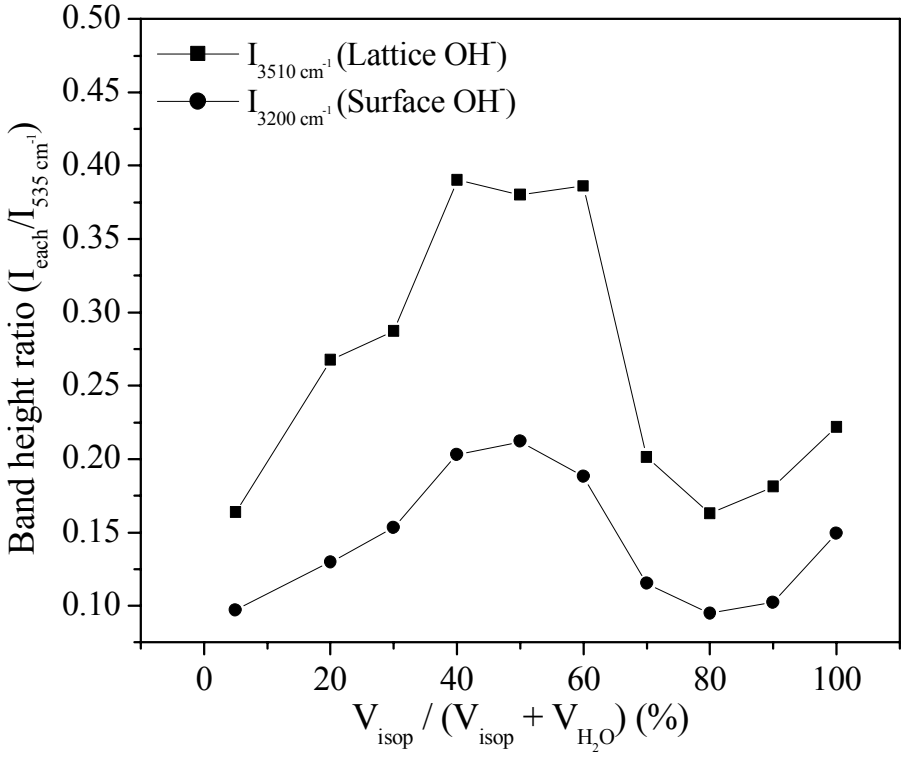

Figure 3.5 Normalized band height ratios of lattice and surface OH^- groups (a) as a function of isopropanol

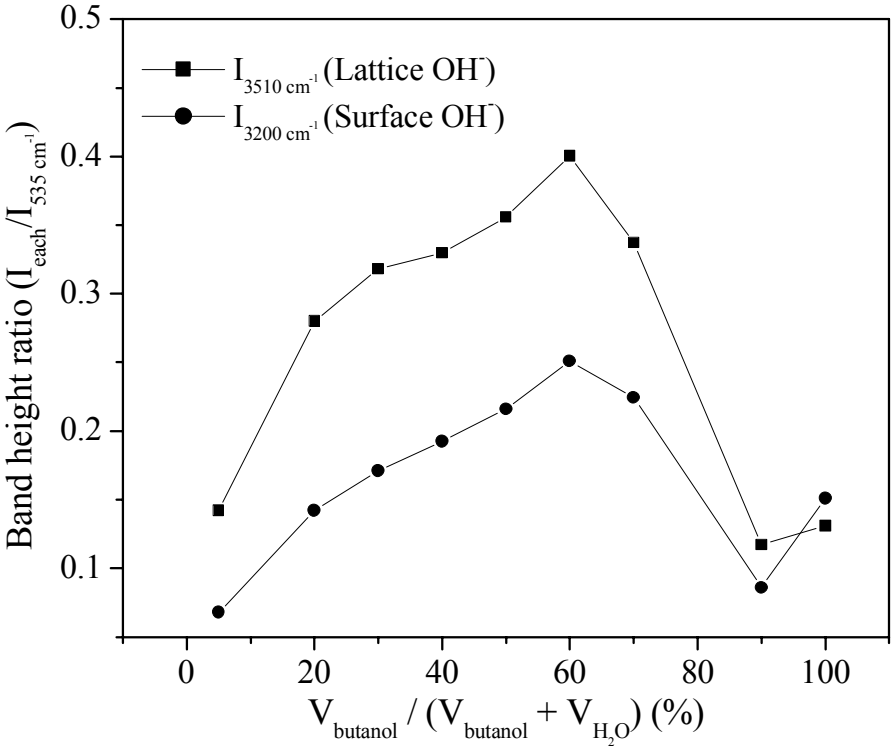

Figure 3.5 Normalized band height ratios of lattice and surface OH^- groups (b) as a function of butanol

3.5. Lattice parameter a-axis

Fig. 3.6 shows the effect of organic solvent composition on the a-axis in the unit lattice. The behavior of the a-axis approximately agreed with that of lattice OH^- content shown in Fig. 3.5. This is because, as mentioned previously, the lattice OH^- groups expand the unit lattice and enlarge the a-axis. Thus, the higher the lattice OH^- content is, the more the lattices expanded.

The lowest a-axis value is recorded at a solvent concentration of around 70-90%, which should indicate that the high concentration of organic solvent or the less polar condition can successfully hinder the OH^- incorporation into the lattices. However, it is seen that the a-axes of the samples synthesized with isopropanol and butanol at 100% organic solvent composition are suddenly enlarged, although a big change in lattice OH^- content between 90 and 100% is not observed as shown in Fig. 3.5. One of the plausible explanations for this a-axis increase at 100vol% is that the samples synthesized at 100vol% can contain some uncrystallized phase, that is, amorphous phase. The value of a-axis is dependent on the position (angle) of a XRD peak. The higher an angle of a XRD peak is, the lower the a-axis is. If the sample contains some amorphous phase, the XRD peak of the sample is the sum of the broad XRD peak associated with the amorphous phase and the sharp peak associated with the crystal phase. Therefore, the resulting peak of the sample can be shifted to a lower angle due to the broad peak of an amorphous phase.

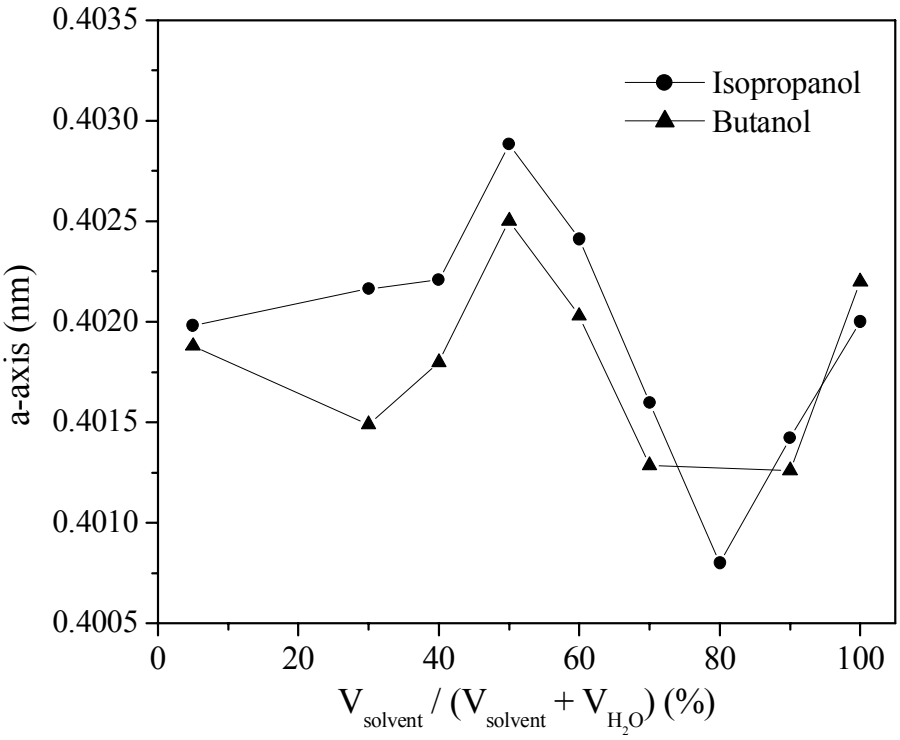

Figure 3.6 Lattice a-axis parameter as function of the solvent composition of isopropanol and butanol

3.6. Dielectric properties

Fig. 3.7 shows that the dielectric properties of $BaTiO_3$ powder synthesized with a different amounts of isopropanol. According to Fig. 3.7, the samples synthesized with around 40 to 60 vol% of isopropanol recorded the lowest dielectric constant. This is because those samples have the largest content of lattice OH^- groups, and the unit lattices are highly expanded as shown in Fig. 3.5 and 3.6, leading to a low dielectric constant. In contrast, since the samples synthesized with 70 to 80 vol% of isopropanol have less OH^- content and a smaller a-axis, their dielectric constant was found to be the greatest.

According to the results in the previous chapter, dielectric loss increased with higher concentration of OH^- groups in a powder. In fact, the largest dielectric loss was observed at 50vol%. This was because the sample synthesized with 50vol% had the highest OH^- content as shown in Fig. 3.5(a). However, it was seen that the dielectric loss at 100vol% drastically increased. This result may support the assumption mentioned in the last section that the sample synthesized at 100vol% can contain an amorphous phase to some extent.

The dielectric constants and losses and the OH^- FT-IR band height ratios of all prepared samples in chapter 2 and 3 and a hydrothermally prepared commercial powder, BT8 (Cabot corp. average particle size; 240nm) are shown in Table 3. Compared to the commercial powder (BT8), the dielectric constant of the ACS samples is about 30% higher at a maximum while the dielectric loss is about 23% is lower. In addition, the concentrations of surface and lattice OH^- groups in the ACS samples are 87 and 79% lower at a maximum, respectively. Therefore, we can say that our WACS and SACS samples are eligible for the applications of MLCCs and embedded capacitors.

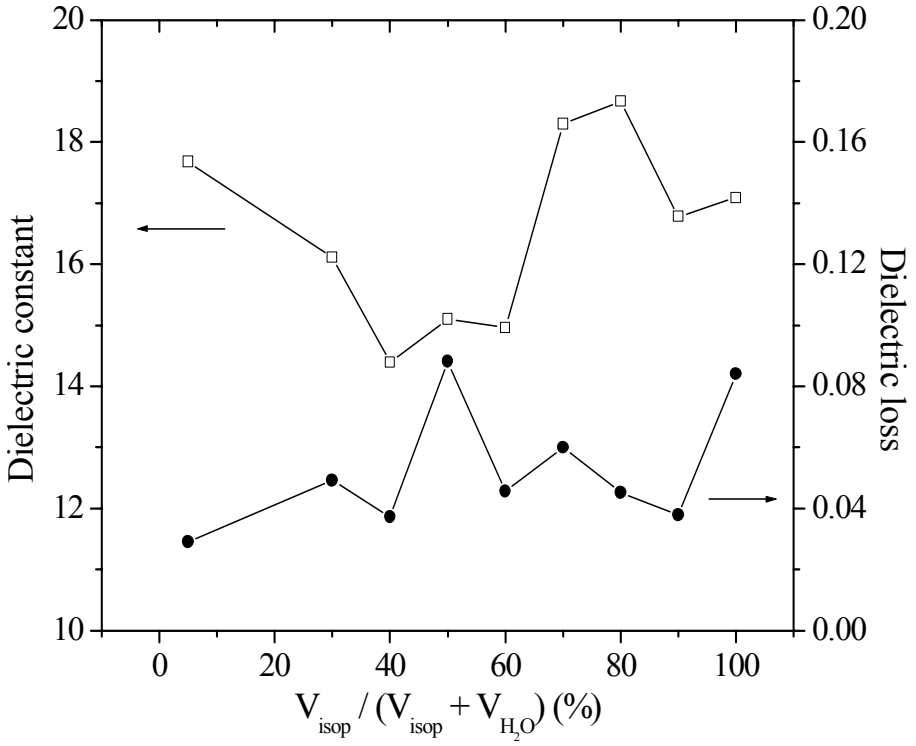

Figure 3.7 Room temperature dielectric constant and loss of a castor oil-matrix composite with 30vol% of $BaTiO_3$ powder synthesized with different amounts of isopropanol

Table 3 The dielectric properties and OH^- FT-IR band ratios of $BaTiO_3$ prepared via a WACS or SACS method and a commercial $BaTiO_3$

Sample name	Surface OH^- ratio	Lattice OH^- ratio	Dielectric constant	Dielectric loss
WACS 1	0.063	0.163	17.6	0.029
WACS 2	0.095	0.199	16.1	0.036
WACS 3	0.116	0.229	16.4	0.041
WACS 4	0.141	0.26	16.4	0.05
WACS 5	0.15	0.271	17.1	0.05
WACS 6	0.155	0.274	17.2	0.058
WACS 7	0.181	0.348	15.7	0.038
WACS 8	0.197	0.369	15.9	0.056
WACS 9	0.252	0.41	16.6	0.082
WACS 10	0.265	0.422	16.8	0.145
WACS 11	0.263	0.441	16.7	0.144
WACS 12	0.276	0.422	16.9	0.135
WACS 13	0.062	0.144	19.2	0.028
WACS 14	0.045	0.107	18.9	0.028
WACS 15	0.041	0.098	19.7	0.027
WACS 16	0.034	0.077	20.4	0.027
SACS 1	0.153	0.287	16.1	0.049
SACS 2	0.203	0.39	14.3	0.037
SACS 3	0.212	0.38	15.1	0.088
SACS 4	0.187	0.385	14.9	0.045
SACS 5	0.115	0.201	18.3	0.06
SACS 6	0.094	0.162	18.6	0.045
SACS 7	0.102	0.181	16.7	0.037
SACS 8	0.149	0.221	17	0.084
BT8	0.268	0.369	15.9	0.035

4. Conclusions

$BaTiO_3$ nano-powders have been successfully synthesized in a mixed solution of water and a different organic solvent under mild conditions. The properties of as-prepared samples were investigated as a function of the organic solvent composition. The crystallite and particle size highly decreased with higher solvent composition. Supersaturation of $BaTiO_3$ increased because of a decrease in the solubility of $BaTiO_3$, resulting in a higher rate of nucleation and smaller crystallite size. The concentrations of lattice and surface OH^- groups in the powder were continuously increased until around 50~60vol% of organic solvent composition, but beyond it both OH^- concentrations rapidly decreased and those were slightly increased between 90 and 100vol%. The change in the a-axis in the unit lattice approximately corresponded with the results of OH^- concentration. The samples with less OH^- content and a lower a-axis tended to show a higher dielectric constant and lower dielectric loss. Compared to a commercial powder (BT8), the WACS and SACS samples showed superior properties in terms of the dielectric properties and the concentration of OH^- groups.

Reference

1. S.G. Kwon, B.H. Park, K. Choi, E.S. Choi, S. Nam, J. W. Kim and J. H. Kim, J. Euro. Ceram. Soc. **26** 1401 (2006)
2. B.I. Lee, X. Wang, S.J. Kwon, H. Maie, R. Kota and J. H. Hwang, J. G.. Park, M. Hu, Microelectron. Eng. **83** 463 (2006)
3. R. Kota, A.F. Ali and B.I. Lee, M.M. Sychov, Microelectron. Eng. (in press)
4. S. Yoon, S. Baik, M.G. Kim and N. Shin, J. Am. Ceram. Soc. **89** 6 1816 (2006)
5. A. Testino, M.T. Buscaglia, M. Viviani, V. Buscaglia and P. Nanni, J. Am. Ceram. Soc. **87** [1] 79 (2004)
6. A. Testino, V. Buscaglia, M.T. Buscaglia, M. Viviani and P. Nanni, Chem. Mater. **17** 5346 (2005)
7. M. Viviani, M.T. Buscaglia, A. Testino, V. Buscaglia, P. Bowen and P. Nanni, J. Euro. Ceram. Soc. **23** 1383 (2003)
8. H. Maie, B.I. Lee, J. Mater. Sci. (in press)
9. N.G. Devaraju, B.I. Lee, M. Viviani, P. Nanni and E.S. Kim, J. Mater. Sci. **41** 3335 (2006)
10. H.I. Chen, H.Y. Chang, Colloids. Surf. A: Physichochem. Eng. Aspects **242** 61 (2004)
11. W. Lu, M. Quilitz, H. Schmidt, J. Euro. Ceram. Soc. (2007)
12. S.K. Patil, N. Shah, F.D. Blum and M.N. Rahaman, J. Mater. Res. **20** 12 (2005)
13. T. Noma, S. Wada, M. Yano and T. Suzuki, J. Appl. Phys. **80** 9 5223 (1996)

14. S. Wada, T. Suzuki and T. Noma, J. Ceram Soc, Jpn. **103** 1220 (1995)

15. S. Wada, H. Yasuno, T. Hoshina, Song-Min Nam, H. Kakemoto and T. Tsurumi, Jpn. J. Appl. Phys. **42** 6188 (2003)

16. S. Wada, M. Narahara, T. Hoshina, H. Kakemoto and T. Tsurumi, J. Mate. Sci. **38** 2655 (2003)

17. G. Busca, V. Buscaglia, M. Leoni and P. Nanni, Chem. Mater. **6** 955 (1994)

18. D.R. Brezinski, An Infrared Spectroscopy Atlas for the Coatings Industry, 4th ed., Blue Bell, 1991, Vol. 1

19. S.W. Lu, B.I. Lee and L.A. Mann, Materials Letters, **43** 102 (2000)

20. B.I. Lee, J. Electroceram. **3** [1] 53 (1999)

21. S. Lu, B.I. Lee, Z, L, Wang and W.D. Samuels, J. Crys. Growth **219** 269 (2000)

CHAPTER 4

PREPARATION AND CHARACERIZATION OF SILVER/BARIUM TITANATE NANOCOMPOSITE POWDER SYNTHESIZED BY AMBIENT CONDITION SOL PROCESS

Abstract

An Ag/$BaTiO_3$ nanocomposite was directly synthesized via an ambient condition sol (ACS) process, using barium nitrate, titanium isopropoxide, and silver nitrate. The properties of the composite powder were studied in relation to temperature of heat-treatment and Ag concentration. XRD results show no reaction products other than Ag and $BaTiO_3$. The $BaTiO_3$ phase was cubic at room temperature. According to SEM micrographs, nearly spherical and well-dispersed $BaTiO_3$ particles with an average particle size of 60nm were observed and Ag particles (< 10nm) were found only on the surface of $BaTiO_3$ particles. The hydroxyl groups existing in the composite were desorbed with increasing calcination temperature between 200 and 700 ^oC. Heat treatment successfully improved the dielectric properties of the composite powder. The dielectric permittivity of the composite powder was highly increased with increasing concentration of Ag while the dielectric loss slightly increased.

1. Introduction

Historically, barium titanate was the first composition used for high-dielectric constant capacitors and is still the industry standard [1]. However, the enhancement of the dielectric properties are highly demanded from ceramic capacitor industries for the preparation of volume-efficiency capacitors. As mentioned earlier, one of the several ways to increase the dielectric properties of dielectric ceramics is to add a conducting phase such as a metal.

Metal/ceramic dielectric composites can be categorized into two generally used types. The first one is the ceramic-matrix composite with metallic filler in a sintered ceramic form. The other is metal/ceramic composite in a powder form, which is used as filler in a polymer matrix. Most of the reported studies on metal/ceramic composite systems mainly dealt with the ceramic-based sintered forms like pellets or thin films. A lot of investigation on their synthesis processes, dielectric properties, mechanical properties, and microstructure are reported. In contrast, the performance, synthesis processes, and characterization of the metal/ferroelectric powder form itself are not well studied. Nevertheless, the use of the powder form has become more important for the application of filler in polymer-matrix embedded capacitors. The materials generally used as filler for this application are either dielectric ceramic or metal powder. However, metal/ceramic particle filled composites are being thought of as a potential candidate now because high dielectric properties can be achieved with relatively low filler-load without a high risk of percolation.

Extensive studies on $Ag/BaTiO_3$ composites in the sintered form have already been carried out in terms of the microstructure, electrical, and mechanical properties [2-8]. In most of the cases to fabricate this composite, a mixture of commercial $BaTiO_3$ powder and silver nitrate in ethanol is ball-milled followed by drying and calcination ($<360^oC$). A direct processing method to simultaneously synthesize fine powders of $BaTiO_3$ and Ag has not been studied.

Considering these backgrounds, this work is aimed to the simultaneous and direct synthesis of both Ag and $BaTiO_3$ nano-powders via ACS method and the investigation on the properties of the composite powders.

2. Experimental

2.1. Powder synthesis

Barium nitrate (Aldrich), titanium isopropoxide (Tyzor TPT), silver nitrate (Alfa Aesar) were used as the starting materials. Nitrates of barium and silver were dissolved together in distilled water at room temperature with stirring to form solution A. Solution B was formed by dissolving titanium isopropoxide in a mixture of acetylacetone and 2-methoxyethanol by stirring. The solution mixture was equipmolar with respect to acetylacetonate and titanium. Solution A was added dropwise to solution B with constant stirring. A series of theses mixtures was prepared keeping the Ba/Ti precursor ratio at 1.1 for all samples while the silver nitrate content was varied to obtain final composite products of 0 to 15vol% of Ag. Each mixed solution was covered with aluminum foil and

kept at 65 ^{o}C for 2 h in a circulating-atmosphere oven and then at 90 ^{o}C for 1.5 h to form a gel. The formed gels were vigorously agitated in their mother liquors before 53ml of 10 molar NaOH solution was slowly added with constant agitation in order to adjust the pH. Each mixture was then placed in a tightly closed 500 ml Teflon jar and kept at 150 ^{o}C for 6 hours in an oil bath. The product solids were repeatedly washed with diluted acetic and then with distilled water to get rid of carbonates, extra barium ions, and all sodium ions. These solids were dried overnight at 70 ^{o}C in a vacuum oven, and the dried lumps were crushed and finely grinded.

2.2. Powder characterization

The as-prepared powders and the heat-treated samples were examined by XRD. Room temperature XRD patterns of Ag/$BaTiO_3$ composites were recorded in the 2θ range of 20^{o} - 80^{o} and 37^{o} - 40^{o} (RTXRD, Scintag PADV using CuKa with λ=0.15406 nm). The microstructure, particle size, and morphology of the $BaTiO_3$ and Ag nanoparticles in the composite powders were investigated by a TEM (Hitachi, HD2000).

The dielectric constants of the powders were determined with the capacitor technique. The capacitor was fabricated using a procedure described in our previous work elsewhere [9,10]. The capacitor technique used consisted of a slurry/paste form with a different volume-fraction of composite powder and castor oil filled in a Teflon-cell with aluminum plate electrodes. Capacitance was measured at 1 MHz using a HP 4284A Precision LCR Meter. The dielectric constant values (K) of the capacitor were calculated

from the measured capacitance data using the equation: [$C = K\varepsilon_o A/T$], where ε_o is the dielectric permittivity of the free space, ($8.854*10^{-12}$ F/m), A is the contact area between the electrode and ceramic paste, ($1cm^2$), and T is the thickness of the specimen, (0.4 cm).

3. Results and Discussion

3.1. Crystal structure

Fig. 4.1(a) shows the room temperature X-ray diffraction patterns of the $BaTiO_3$/Ag powders with 5vol% of Ag treated at different calcination temperatures. The diffraction peaks indicated that no phases other than $BaTiO_3$ and Ag are detected. It is clear that $BaTiO_3$ and Ag were individually formed without any interaction between them during the ACS process and subsequent calcination. The crystal structure of $BaTiO_3$ was assigned to the cubic phase as the (200) and (002) peaks around $2\theta = 44.95^o$ are not split. Although the (111) peak of Ag appear to partially overlap with that of $BaTiO_3$ in Fig. 4.1(a), Ag metal was successfully formed even before the calcination step. This result indicated that a processing temperature as low as 150 ^oC, used in the wet chemical step, was enough for the crystallization of the Ag phase.

As the calcination temperature increased, the XRD peaks of Ag intensified and sharpened because the crystallization of silver was highly promoted by the calcination. On the contrary, the effect of calcination on the peaks of $BaTiO_3$ was seen more in terms of peak-shift rather than intensity of the peaks. Fig. 4.1(b) shows that the (111) peak of $BaTiO_3$ was shifted toward higher angles as calcination temperature increased. This peak

shift is associated with the shrinkage of the lattice parameter, a-axis, of $BaTiO_3$ in the composite. The lattice unit of $BaTiO_3$ in the composite expands if hydroxyl groups, OH^-, are present in the lattice. Since calcination eliminates the OH^- groups from the lattice, shrinkage along the a-axis occurred. Fig. 4.1(b) shows that the room temperature lattice parameter a-axis of $BaTiO_3$ in the composite, calculated based on the $BaTiO_3$ (111) peak position, contracted from 4.027 to 3.998Å in the calcination temperature range between RT and 700^{o}C. This implies that OH^- groups were successfully eliminated. The role and elimination of OH^- groups in the composite will be discussed with the FT-IR data below. Fig. 4.1(c) shows the XRD patterns of pure $BaTiO_3$ and Ag/$BaTiO_3$ composites having different volume ratios of Ag calcined at 550^{o}C for 7 h. It is obvious that the XRD peak intensity of Ag metal increased with the increase in vol% of Ag.

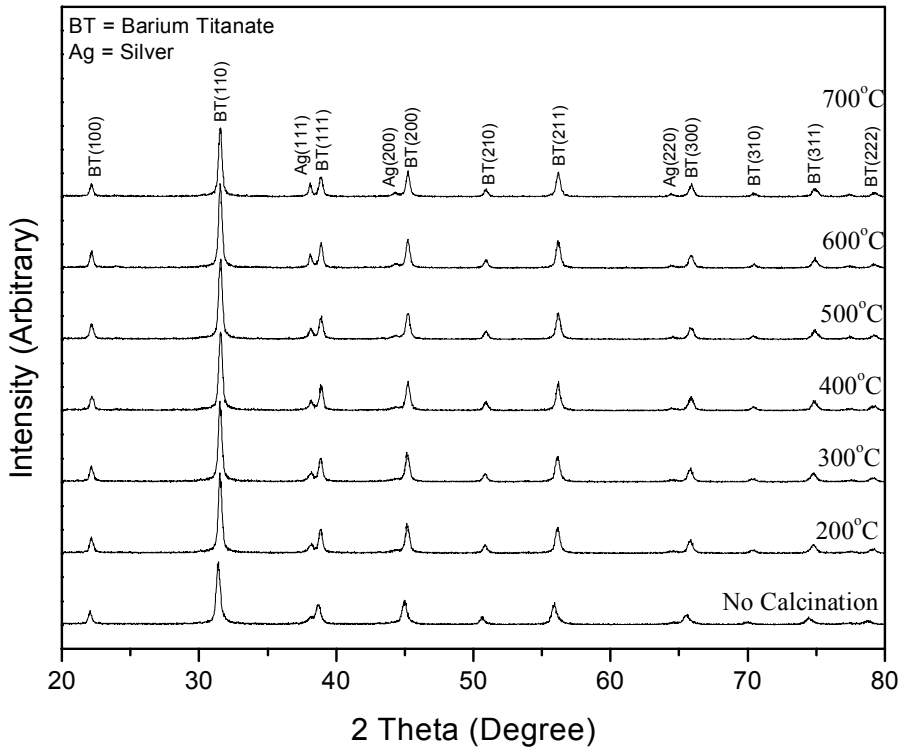

Figure 4.1(a) XRD patterns of $Ag/BaTiO_3$ powder with 5 vol% silver calcined at different calcination temperatures for 5 hrs

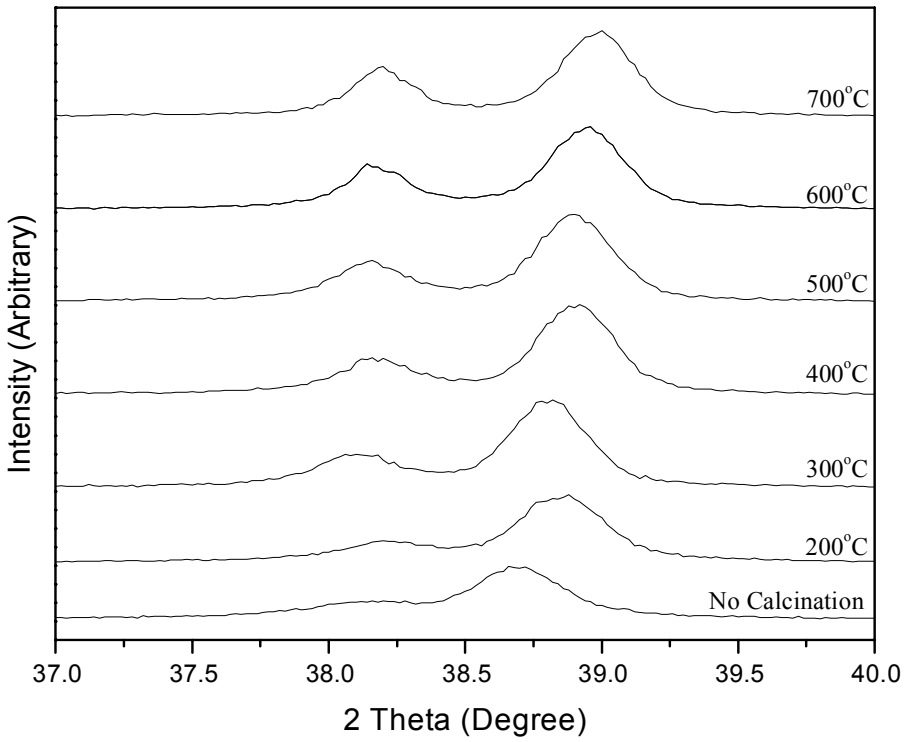

Figure 4.1(b) Enlargement of Fig. 1(a) indicating the peak shift of $BaTiO_3$

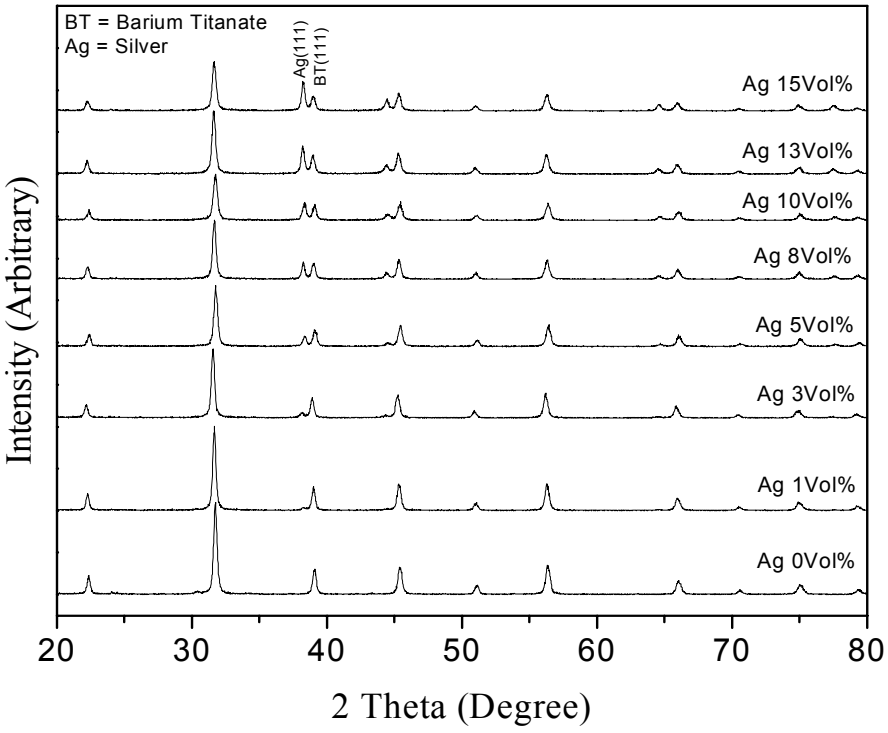

Figure 4.1(c) XRD patterns of $Ag/BaTiO_3$ powder calcined at 550^{o}C for 7 h with different vol% of Ag

3.2. Morphology

Fig. 4.2 shows the SEM micrographs of $BaTiO_3$ particles with no Ag content calcined at 550 ^oC and $Ag/BaTiO_3$ composite particles with 15vol% of Ag calcined at 550^oC. According to Fig. 4.2(a), homogeneously dispersed $BaTiO_3$ powder with a nearly spherical shape and little agglomeration was seen. The average $BaTiO_3$ particle size, estimated from SEM data, was around 60nm. On the other hand, finer Ag particles (<10nm) with spherical shape are found only on the surface of $BaTiO_3$ particles as shown in Fig. 4.2(b). It can be assumed that Ag particles were mainly formed through a reduction and aggregation process. The Ag^+ ions were homogeneously dispersed in the starting precursor solution, and then in the ACS process of heating at 150^oC under the closed condition, the Ag ions were reduced into Ag metal. The continuous heating and the following calcination process led to the aggregation of Ag. This aggregation process, however, is not strong in this system, resulting in the formation of small and well-dispersed Ag particles. In addition, Chen et al [11,12] reported that the solubility of Ag in $BaTiO_3$ is negligible since the lattice parameters in sintered $BaTiO_3$, such as the a-axis and c-axis, and the Curie temperature are not affected by addition of Ag. Therefore, it can be assumed that contact of $BaTiO_3$ with Ag particles has no interaction. The size of $BaTiO_3$ particles depends on the synthesis conditions such as the concentration of Ba^{2+}, temperature, Ba/Ti ratio, basicity (pH), and precursor concentrations [13,14]. In general, higher Ba^{2+}, Ba/Ti ratio, and pH facilitate the production of smaller $BaTiO_3$ particles [15-17]. Therefore, it should also be possible for this method to control the particle size of

$BaTiO_3$ powder from nano to submicron size by changing the synthesis parameter, as there is no interaction between $BaTiO_3$ and Ag during the synthesis.

3.3. Impurity

The content of OH^- groups in the composite powders were investigated. Since the hydroxyl ions impart an adverse effect on the dielectric properties of $BaTiO_3$, it should be important to know how much OH^- groups are present in each composite powder in evaluating their effect on the dielectric properties. Using the FT-IR baseline method [18], a semi-quantitative FT-IR analysis, the peak height ratios of I_{3200}/I_{535} and I_{3500}/I_{535} were used to estimate the relative content of both surface and lattice OH^- in $BaTiO_3$ particles. According to Fig. 4.3, it was seen that, as the calcination temperature increased, the peak height ratios decreased, indicating desorption of OH^- groups. This result supports the idea that removal of lattice OH^- groups resulted in shrinkage of $BaTiO_3$ lattice a-axis, as shown above (the shrinkage of a-axis from 4.027 to 3.998Å).

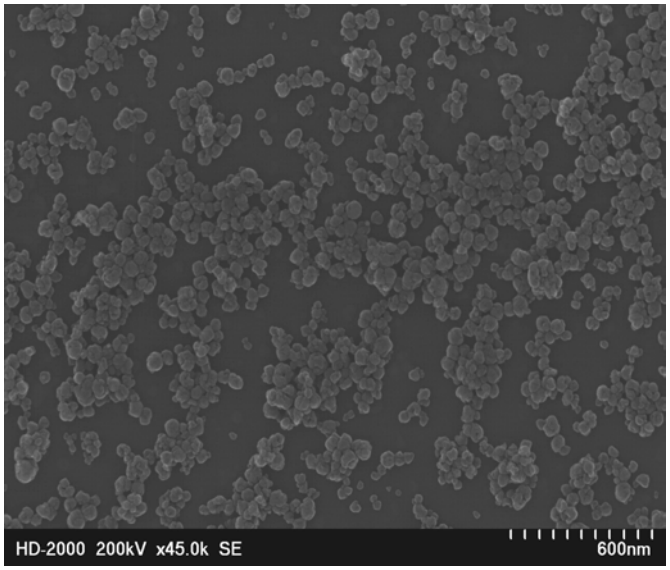

(a)

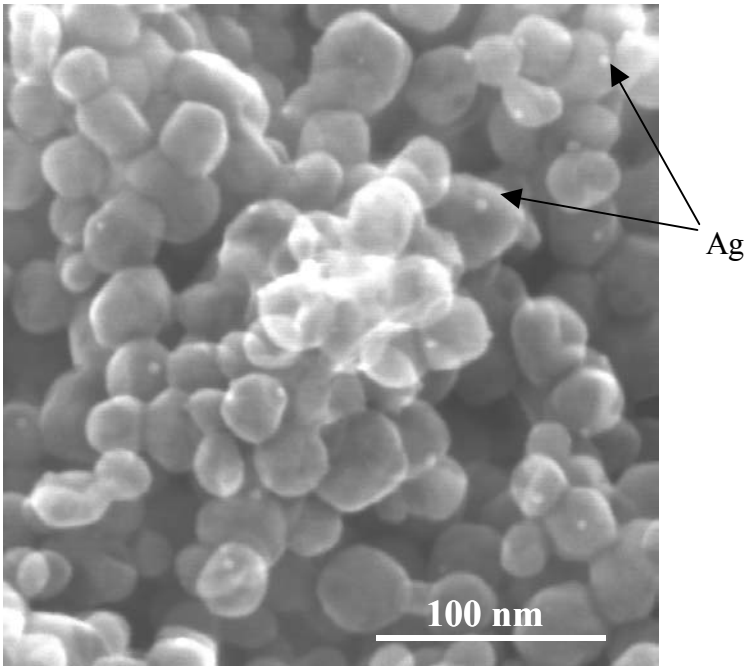

(b)

Figure 4.2 SEM micrographs of (a) the $BaTiO_3$ particles with no Ag content calcined at 550 ^oC (b) Ag/ $BaTiO_3$ particles with 15 vol% of Ag calcined at 550 ^oC

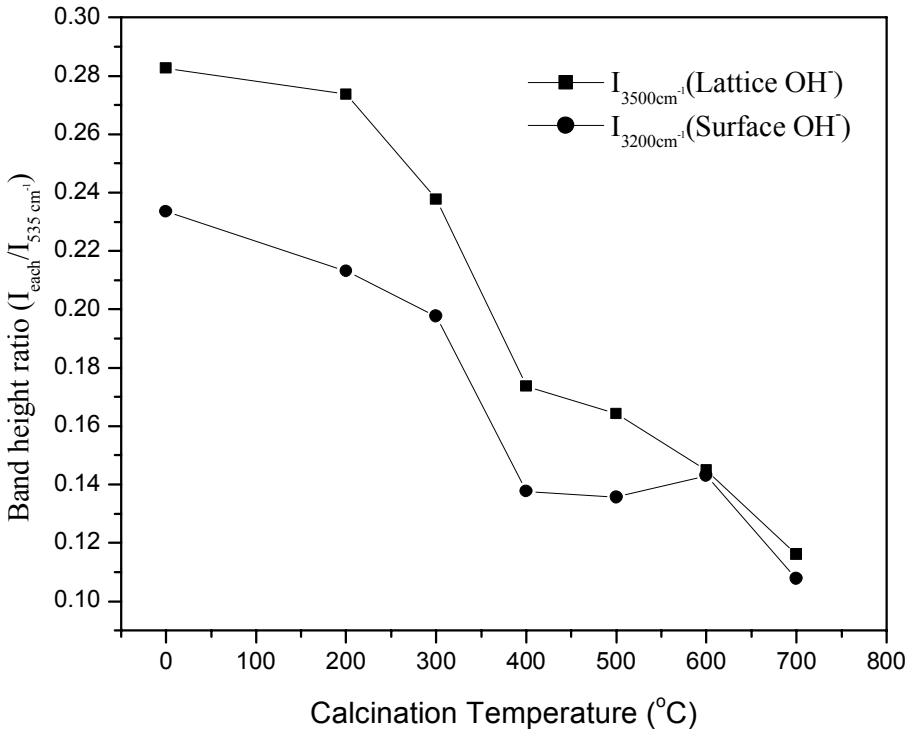

Figure 4.3 Calculated peak ratio of lattice and surface OH groups in $BaTiO_3$ powder as a function of calcination temperature from the FT-IR spectra

3.4. Dielectric properties

Fig. 4.4 shows the room temperature dielectric properties of a castor oil-matrix Ag/$BaTiO_3$ composite with 5vol% of Ag calcined at different temperatures. It shows that the dielectric constant of the ACS derived nano-composite powder highly increased and the dielectric loss decreased with higher calcination temperature. According to our previous work, this improvement of the dielectric properties should be explained by the reduction of OH^- groups for each calcined composite and elimination of pores existing around the particles. In addition, the high increase in the dielectric constant recorded at a calcination temperature between 600 and 700^oC should be rather related to the recovery of tetragonality in $BaTiO_3$. The cubic lattice parameter, a-axis, of $BaTiO_3$ in the composite calcined at 700^oC was 3.998Å. This is lower than the expected lattice parameter for defect-free cubic $BaTiO_3$, and this implies the crystal structure of $BaTiO_3$ in the composite calcined at 700 ^oC is partially tetragonal.

Fig. 4.5 shows the room temperature dielectric constants of castor oil-matrix Ag/$BaTiO_3$ composites calcined at 550^oC for 7 h as a function of Ag concentration. The dielectric constant is highly improved with an increase in Ag content while the dielectric loss is only slightly increased.

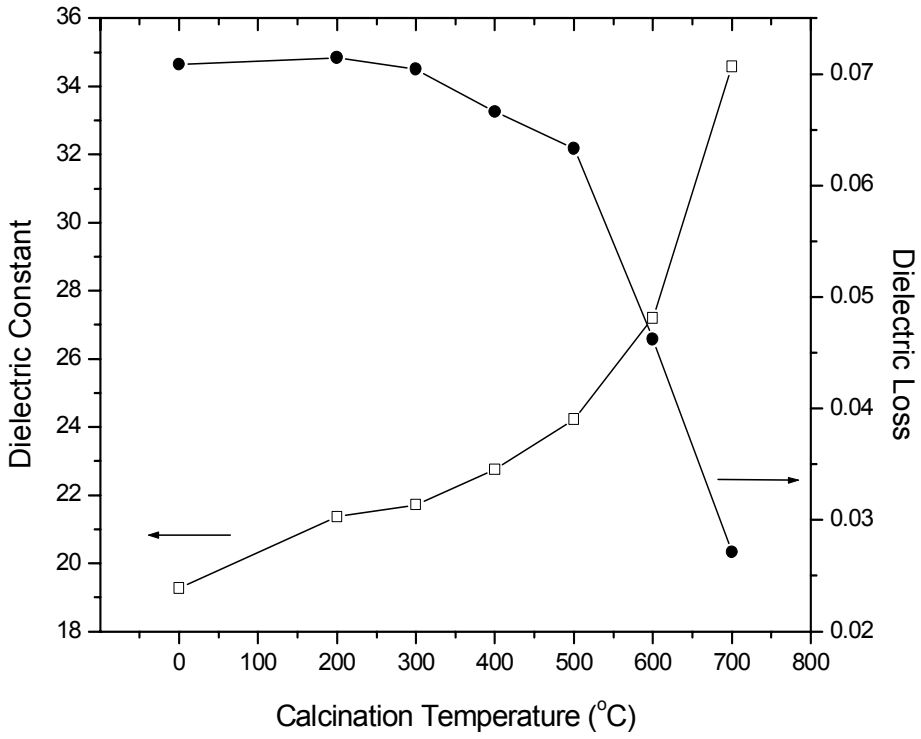

Figure 4.4 Room temperature dielectric constant and loss of castor oil-matrix $Ag/BaTiO_3$ composite with 30vol% of $Ag/BaTiO_3$ powder as a function of calcination temperature between 0 and 700 °C

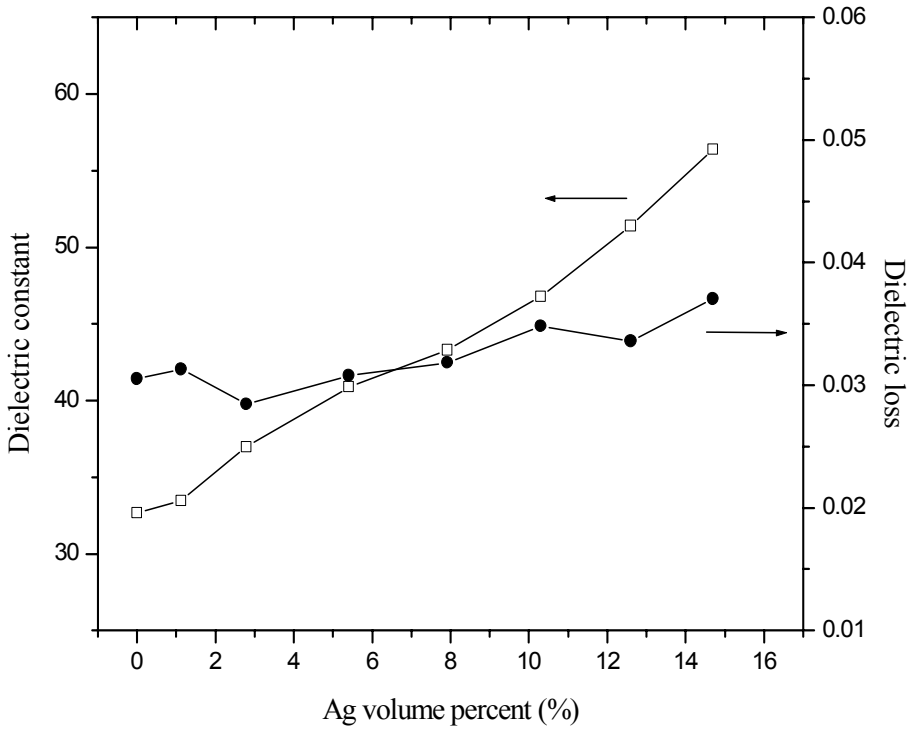

Figure 4.5 Room temperature dielectric constants and loss of castor oil-matrix $Ag/BaTiO_3$ composite with $Ag/BaTiO_3$ powders calcined at 550^oC as a function of Ag concentration

4. Conclusions

$Ag/BaTiO_3$ nano-composite powders have been successfully synthesized by the ACS process. XRD results show no reaction products other than Ag and $BaTiO_3$. The $BaTiO_3$ phase was cubic at room temperature. According to SEM micrographs, nearly spherical and well-dispersed $BaTiO_3$ particles with an average particle size of 60nm were observed and Ag particles (< 10nm) were found only on the surface of $BaTiO_3$ particles. The hydroxyl groups existing in the composite were desorbed with increasing calcination temperature between 200 and 700 ^oC. Heat treatment successfully improved the dielectric properties of the composite powder. The dielectric permitivity of the composite powder was highly increased with increasing concentration of Ag while the dielectric loss slightly increased.

Reference

1. "Ceramic Materials for Electonics: Processing, Properties and Applications" edited by R. C. Buchanan, Marcel Dekker Inc.
2. C. Y. Chen, W. H. Tuan, J. Am. Soc. **83** 12 2988 (2000)
3. C. Y. Chen, W. H. Tuan J. Mater. Sci. Let. **18** 353 (1999)
4. RenZheng Chen, Xiaohui Wang, ZhiLun Gui, LongTu Li, J. Am. Ceram. Soc. 86 6 1022 (2003)
5. S. Panteny, C. R. Bowen, R. Stevens, J. Mater. Sci. **41** 3837 (2006)
6. B.I. Lee, P. Badheka, D.H. Yoon, V. Magadala, M. Wang, J. Ceram. Proc. Res. **5** 2 127 (2004)
7. N. Halder, A. Das Sharma, S. K. Khan, A. Sen, H. S. Maiti, Mater. Res. Bull. **34** 544 (1999)
8. Ji Zhou, Longtu Li, Zhilun Gui, Xiaowen Zhang, D. J, Barber. NanoStruc. Mater. **8** 3 321 (1997)
9. B. I. Lee, X. Wang, S. J. Kwon, H. Maie, R. Kota, J. J. Hwang, J. G. Park, M. Hu., Microelectron. Eng. **83** 463 (2006)
10. R. Kota, A. F. Ali, B. I. Lee, M. M. Sychov, Microelectron. Eng. (submitted)
11. C. Y. Chen, W. H. Tuan, J. Am. Soc. **83** 12 2988 (2000)
12. C. Y. Chen, W. H. Tuan J. Mater. Sci. Let. **18** 353 (1999)
13. Andrea Testino, Maria Teresa Buscaglia, Massimo Viviani, Vincenzo Buscaglia, Paolo Nanni, J. Am. Ceram. Soc. **87** [1] 79 (2004)

14. Andrea Testino, Vincenzo Buscaglia, Maria Teresa Buscaglia, Massimo Viviani, Paolo Nanni, Chem. Mater. **17** 5346 (2005)

15. X. Wang, B. I. Lee, M. Hu, E. A. Payzant, D. A. Blom, Ceram. Transac. **148** 21 (2004)

16. M. Viviani, M. T. Buscaglia, A. Testino, V. Buscaglia, P. Bowen, P. Nanni, J. Euro. Ceram. Soc. **23** 1383 (2003)

17. N. G. Devaraju, B. I. Lee, X. Wang, M. Viviani, P. Nanni, J. Mate. Sci. **41** [11] 3335 (2006)

18. S. W. Lu, B. I. Lee and L. A. Mann, Materials Letters, **43** 102 (2000)

CHAPTER 5

SUMMARY & CONCLUSIONS

In this work, nanocrystalline $BaTiO_3$ and $Ag/BaTiO_3$ particles were successfully synthesized via the ACS process. The resulting powders were characterized in terms of crystal structure, the crystallite and particle size, morphology, the lattice parameter a-axis, the content of the lattice and surface OH^-, particle formation process, and dielectric properties.

Based on the results and discussion presented in this thesis, the following summaries or conclusions can be drawn:

1. Pure $BaTiO_3$ powders with a particle size <100nm and high content of cubic phase could be prepared by using water or a mixed solvent of water and an organic solvent with the WACS and SACS process.
2. Higher $[Ba^{2+}]$ and base concentrations lead to smaller crystallite and particle size due to the higher nucleation rate and higher concentration of OH^- groups in the powder lattices. Longer reaction time formed larger particles due to the aggregation of smaller particles and decreased the concentration of OH^- groups.
3. The reduction of lattice OH^- with longer reaction time contributed to an increase in tetragonality, which increased the dielectric constant. The dielectric constant highly depends on the tetragonality in the powder.

4. The dielectric constant and tetragonality increased below a lattice OH^- concentration of around 0.35 wt%, and above this concentration, both of them were almost kept constant.
5. Heat treatment improved the dielectric properties by the elimination of the pores and desorption of OH^- groups from the powder.
6. The crystallite and particle size of the powders synthesized via SACS decreased with higher organic solvent amount.
7. Although the solubility or dissociation of starting reactants decreased with higher organic solvent amount, the solubility of $BaTiO_3$ also decreased. The resulting higher supersaturation led to a higher nucleation rate and smaller particle and crystallite size.
8. The concentrations of lattice and surface OH^- groups in the powder were continuously increased until around 50~60vol% of organic solvent composition, but beyond it, both concentrations rapidly decreased. They were slightly increased between 90 and 100vol%. The change in a-axis in the unit lattice approximately agreed with the result of OH^- concentration.
9. At high solvent compositions of around 70-80vol%, the lattice OH^- content and the a-axis were recorded as the lowest value, leading to superior dielectric properties.
10. Compared to the hydrothermally prepared commercial powder (BT8), the dielectric constant of the ACS samples is about 30% higher at a maximum

while the dielectric loss is about 23% is lower. In addition, the concentrations of surface and lattice OH^- groups in the ACS samples are about 87 and 79% lower at a maximum, respectively. The ACS samples showed the superior properties in terms of the dielectric properties and the concentration of OH^- groups. The ACS $BaTiO_3$ powders should contribute to the development of MLCCs and embedded capacitors.

11. Pure Ag/$BaTiO_3$ nano-composite powders were directly prepared by the ACS process. Other products were not detected, according to XRD results.
12. The $BaTiO_3$ powders with a nearly spherical shape and a particle size of around 60nm were homogeneously dispersed. On the other hand, finer Ag particles (<10nm) with spherical shape are found only on the surface of $BaTiO_3$ particles.
13. Heat treatment improved the dielectric properties. Higher calcination temperature led to a higher dielectric constant and lower dielectric loss. In addition, the dielectric constant of the powder highly increased with higher concentration of Ag while the dielectric loss only slightly increased.